epic-TN-TC-2025-001

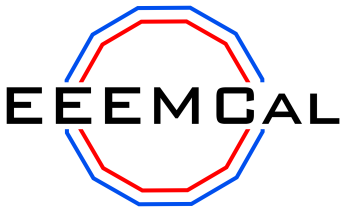

EIC — ePIC — EEEMCal

Design, Assembly, Integration & Installation of the backward ECal

Mechanical Design Report

Julien Bettane

Mechanical engineer

Laboratoire de Physique des deux Infinis Irène Joliot-Curie (IJCLab)
CNRS — IN2P3 — Université Paris-Saclay

on behalf of the ePIC Backward ECal Subsystem Collaboration

March 2025

Contents

1 Introduction

The Electron Endcap Electromagnetic Calorimeter (EEEMCal), designed for integration into the Electron-Proton/Ion Collider (ePIC) experiment at Brookhaven National Laboratory (BNL), represents an important component for the detection and analysis of particles. This document provides an overview of the mechanical design, integration, and installation of the system, focusing on the specific requirements that ensure optimal performance within the challenging environment of the experiment.

Firstly, we will discuss the essential components of the calorimeter, detailing the technical requirements and clearances necessary to ensure a reliable operation. The configuration of the crystals and their arrangement are critical for maximizing the sensitivity and efficiency of the detector. We will also explore aspects related to cooling, including system specifications, ANSYS simulations, and thermal analyses conducted on a 5×5 prototype.

Next, we will describe the mechanical structure, emphasizing the internal and external designs of the cooling system, as well as the associated mechanical calculations. The assembly of the calorimeter will be discussed, including the procedures to be followed, the list of materials, and the resources required to ensure successful integration. We will highlight the essential integration tests necessary to validate the overall functionality of the system.

Finally, the section on transportation and installation will outline the procedures in place to ensure the safe and efficient handling of the calorimeter upon its arrival at BNL, while adhering to mechanical requirements and anticipating challenges related to integration with other systems (services, cooling, electronics).

The development of this project is based on a collaborative and multidisciplinary approach aimed at ensuring compliance with safety standards and best engineering practices. By articulating design, integration, and installation, this document seeks to provide a comprehensive understanding of the technical challenges and the solutions adopted for the EEEMCal calorimeter.

2 Overview and components

2.1 Requirements

The main requirements for the mechanical design can be divided into two sections: the positioning of the crystals and maintaining their temperature stability.

For the crystals, the primary challenge is to place as many crystals as possible close to the beam pipe (respecting the clearance requirements) and to maximize the number of crystals at the external diameter (again considering the clearances). The space between the crystals must be minimized, aiming to strike a balance between achieving precise mechanical assembly and ensuring optimal performance for physics.

Regarding temperature, we must ensure stability within ± 0.1 °C for the crystals (1σ standard deviation). Although temperature gradients along the three axes are not critical to the design, we will still aim to reduce them, targeting a maximum gradient of 2 ° C (this value may change depending on the results of the thermal tests).

Table 1: PWO mechanical properties [3]

Parameters	Values	Units
Density	8.28	$g.cm^{-3}$
Radiation length	0.89	cm
Hygroscopic	No	
Structure	Tetragonal	
Specific heat	263-440	$J.kg^{-1}.K^{-1}$
Thermal conductivity	3300	$W.K^{-1}$
K[001]	2	$W.m^{-1}.K^{-1}$
K[010]	2.4	$W.m^{-1}.K^{-1}$
K[100]	2.4	$W.m^{-1}.K^{-1}$
Mechanical properties	Anisotrope	
Hardness	4	Mohs
Young's modulus (a-plane)	70	GPa
Young's modulus (c-plane)	89	GPa
Fracture strength	27-32	MPa
Normal to [011]	18.5	MPa

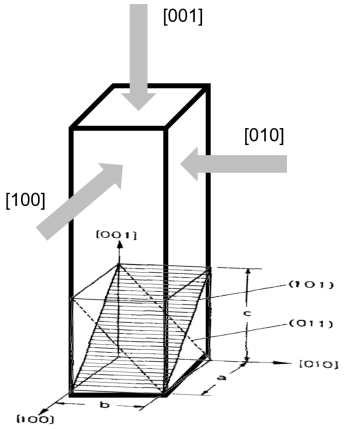

Loading direction	Tensile direction	Fracture strength (Mpa)
[100]	[010]	26,8
[001]	[010]	31,7
[100]	[001]	31,6
[010]	[001]	30,1
// to [011]	⊥ to [011]	18,5

Figure 1: PWO Fracture strength [4]

2.2 PWO Crystals

Based on extensive simulation studies [1], the preferred material for the EEEMCal radiator is lead tungstate (PWO), an extremely fast, compact, and radiation-hard scintillator providing sufficient luminescence yield (15–25 photoelectrons/MeV) to achieve good energy resolution. PWO has been the material of choice for precision electromagnetic calorimeters at JLab, PANDA/GSI, as well as the CMS experiment at the LHC. Achieving good energy resolution, including the so-called constant term, typically requires 20 or more radiation lengths (X_0). The transverse block dimensions are matched to its Molière radius to capture the major part of the transverse shower. The technology for mass production of PWO crystals that guarantees the needed homogeneity of the whole calorimeter has been well established experimentally, most recently with the Neutral Particle Spectrometer [2] at JLab (Fig. 7 in section 2.4).

All the parameters required for the mechanical design are summarized in Table 1 and Figure 1.

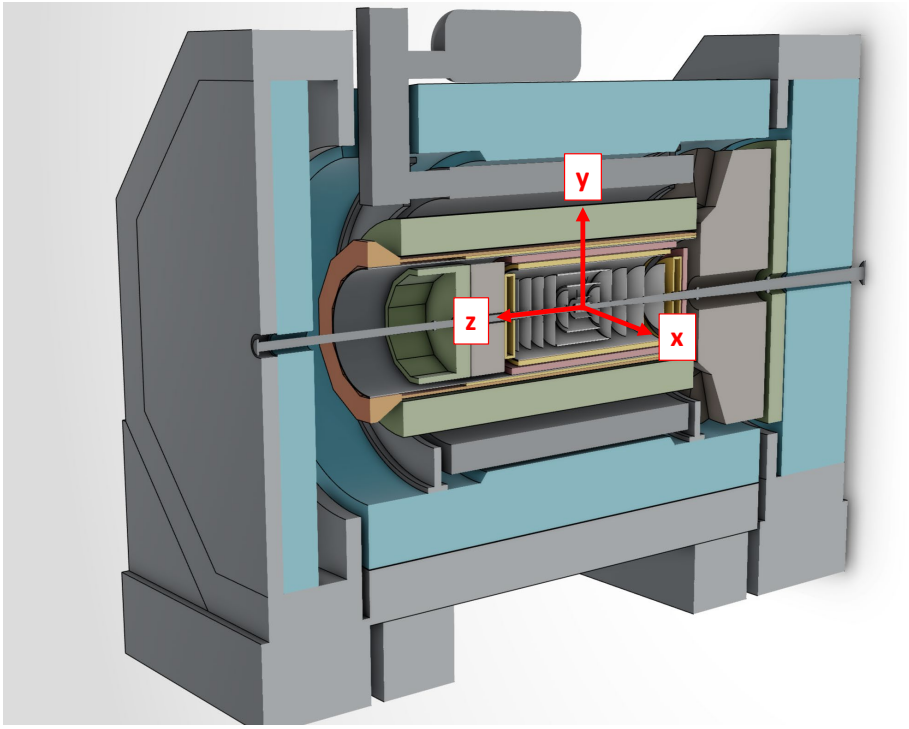

Figure 2: Axis orientation in ePIC

2.3 Clearances

2.3.1 Main components close to the EEEMCal

The detector must be inserted into a carbon tube, requiring careful consideration of clearance for services such as cables and cooling. Additionally, the front face of the EEEMCal must be positioned at a precise distance from the interaction point, ensuring optimal physics performance. At the same time, it is crucial to maintain clearance with the pfRICH detector to prevent mechanical interferences and allow proper integration within the overall experimental setup.

2.3.2 Axis orientation

To facilitate exchanges with other subdetectors, the orientation of the axes has been defined as shown in Figure 2. All clearances and mechanical calculations must be carried out following this axis configuration to ensure consistency across the different subsystems. This standardized orientation will help streamline integration efforts and simplify communication between teams working on different parts of the detector system.

2.3.3 In the plane (x,y)

To ensure proper installation, we must maintain a clearance between the EEEMCal and the surrounding subdetectors, specifically the carbon tube encasing the calorimeter and the beam pipe. Regarding the positioning of the EEEMCal along the beam axis, we must also ensure adequate clearance with the pfRICH detector.

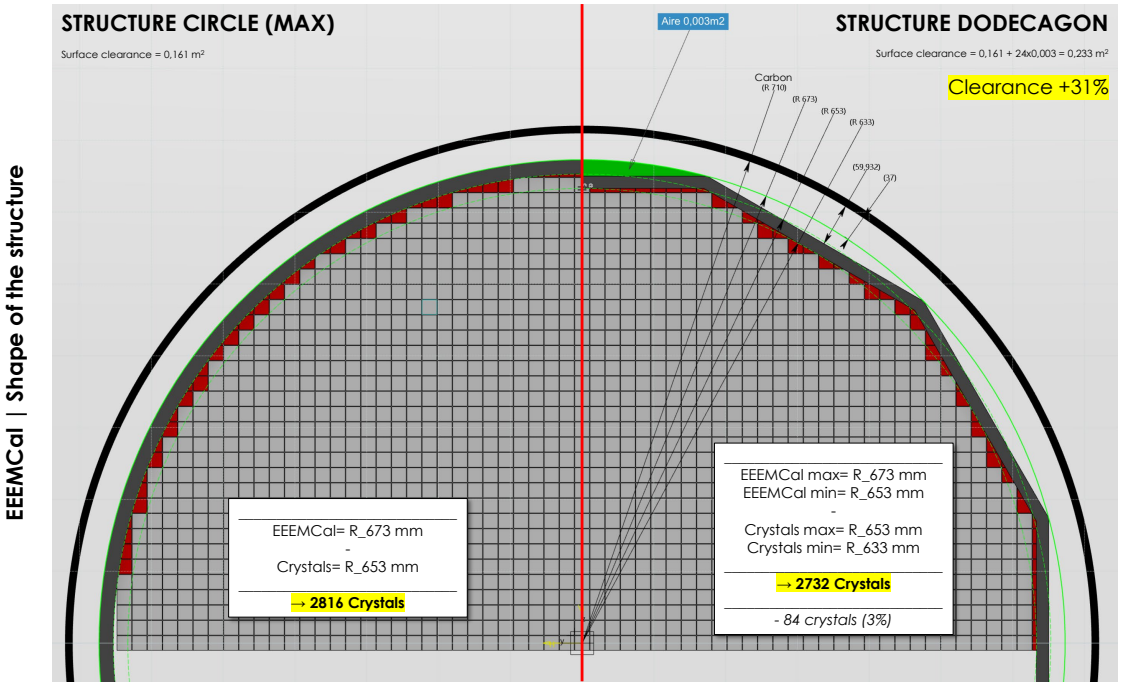

Figure 3: Comparison and main external parameters for the design

- With the radius of the beam pipe = 5 mm (mechanical structure and deflection included)
- With the radius of carbon tube = 37 mm (mechanical structure and deflection included)
- Internal diameter of the carbon tube = 1420 mm
- Diameter max of the EEEMCal = 1346 mm (mechanical structure and deflection included)
- Diameter max of the crystals D= 1306 mm
- Space for the services = 0.233 m^2
- Shape: DODECAGON

Two options were considered: one circular and another with a dodecagonal shape. Results from physics simulations show that the reduction in the number of crystals on the outer diameter does not significantly affect the acceptance and efficiency of the detector [5]. On the other hand, the space required for the services is better accommodated with the dodecagonal shape.

The comparison of the two shapes and the main parameters for the mechanical design of the external part of the detector are shown in the Figure 3.

The drawing of the beampipe used for the design comes from a CAD step file sent by BNL [step file "Beampipe 2023.06.26" and "EPIC Envelope - 01-30-2025.pdf", Roland Wimmer (BNL)]. The file is available on Vault inventor. The dimensions are considered as validated. Any changes will be communicated by BNL. The chosen dimensions in Figure 4 have been validated with BNL, with the chief engineer.

A recent upgrade in the flange design has led to a reduction in the external diameter, improving the available space around the beam pipe. As a result, the clearance between the internal structure and the flange of the beam pipe is now 8 mm [6]. Despite this modification, the overall design of the EEEMCal remains unchanged, ensuring compatibility with previous integration constraints and performance requirements.

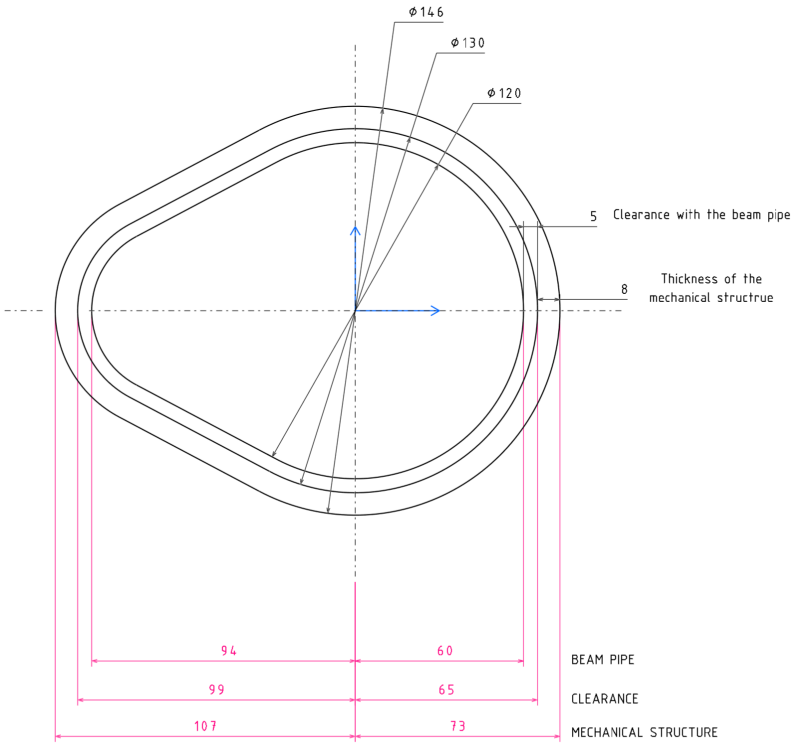

Figure 4: Chosen dimensions around to the beam-pipe flange.

2.3.4 In z axis

The distance between the EEEMCal and the interaction point is 174 cm [7] as explained with the Figure 6. This length includes the mechanical structure, meaning the distance between the front face of the crystals and the interaction point is actually larger. The file "EPIC Envelope - 01-30-2025" contains a summary of all the clearances for the different subdetectors. This document serves as a reference to ensure proper integration and alignment of each component within the overall detector assembly. Figure 5 illustrates the clearances in all directions for the EEEMCal, ensuring that its positioning respects the necessary spatial constraints within the detector setup.

The actual distance between the crystals and the interaction point depends on the mechanical design at the front of the detector, which consists of a grid and a cooling plate. The current design assumes a 20 mm offset. The mechanical technology used for the cooling system directly impacts the required distance for the physics (174 cm), with the worst-case scenario—using copper tubes—potentially increasing the space needed up to 50 mm. This variation highlights the need for further validation through prototypes, which will help assess the feasibility of different cooling solutions and refine the final design. By testing these prototypes, the team can determine the most efficient and space-saving cooling approach. Therefore, the estimated distance between the crystals and the interaction point is between 176 cm and 179 cm.

The clearance between the EEEMCal and the pfRICH detector is 15 mm, accounting for both the mechanical structure and the necessary cabling. This limited space requires careful planning to ensure proper integration without interference between the two detectors. Special attention must be given to the routing of cables and mechanical supports to optimize the available space

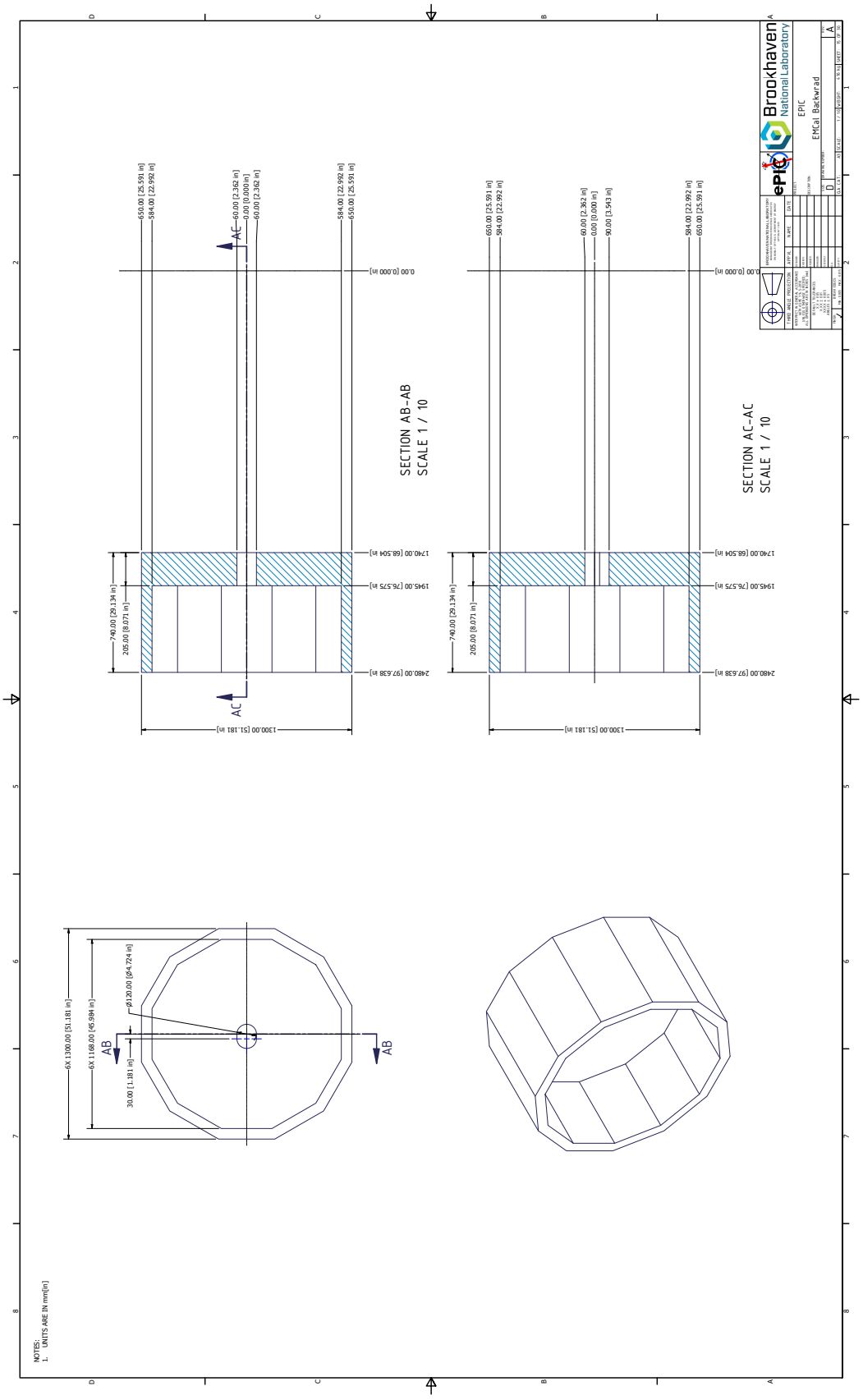

Figure 5: Clearances for the EEEMCal in all directions

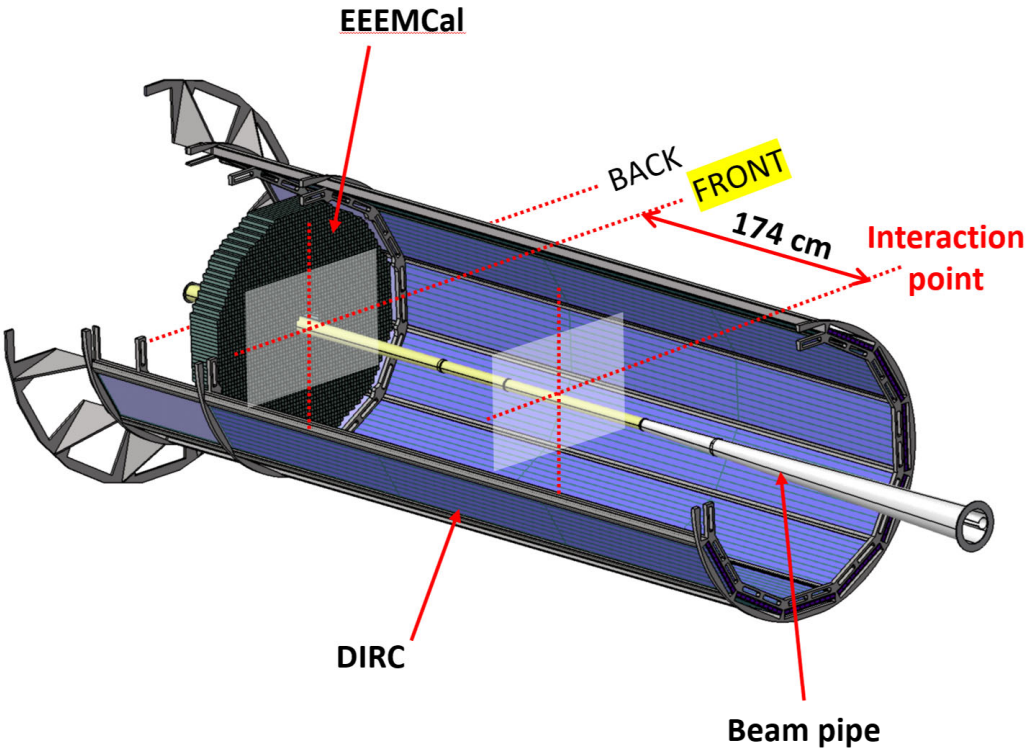

Figure 6: Positioning of the EEEMCal into the ePIC detector. The distance d between the interaction point and the front face of the crystals is 176 cm $< d <$ 179 cm (the ideal position in terms of physics performance is 174 cm).

Table 2: Values of the main clearances for the EEEMCal

Clearance With	Values	Units	Comments
Carbon tube	37	mm	Mechanical structure and deflection included
Beam pipe	5	mm	Mechanical structure and deflection included
Services	0.233	m^2	Total= 0.161 + 12×0.006 = 0.233 m^2
pfRICH	15	mm	Mechanical structure and deflection included
Interaction point	174	cm	Mechanical structure and deflection included
Carbone tube Diameter	1420	mm	Internal limit
EEEMCal Diameter	1346	mm	External limit
Dodecagon side	348.35	mm	Inscribed in the Diameter

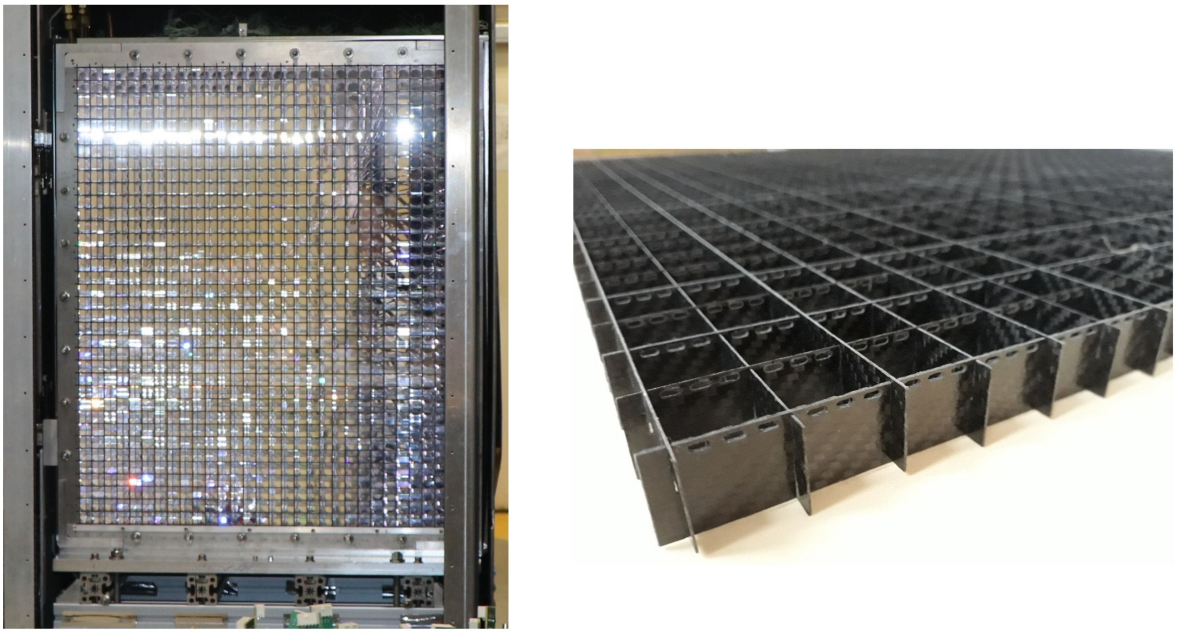

Figure 7: NPS calorimeter installed in the Hall C of Jefferson Lab

while maintaining accessibility for installation and maintenance. Ensuring that this clearance is respected is essential to avoid mechanical conflicts and to guarantee the smooth operation of both detectors within the system.

2.4 Wrapping and space between crystals

The wrapping consists of a reflective material combined with a light-isolating material. The current space between each crystal is 0.76 mm. This choice is based on the same mechanical design used for the NPS calorimeter, which was operated at Jefferson Lab in 2023–2024 (Figure 7). We plan to test several thicknesses for the carbon plates placed between the crystals.

- Reflector : ESR "VM2000", Enhanced Specular Reflector® (3M) = 0.65 μm thickness
- Light insulation : Tedlar® (DuPont) = 0.65 μm thickness
- Thickness of the carbon plate = 0.3 mm $< t <$ 0.5 mm

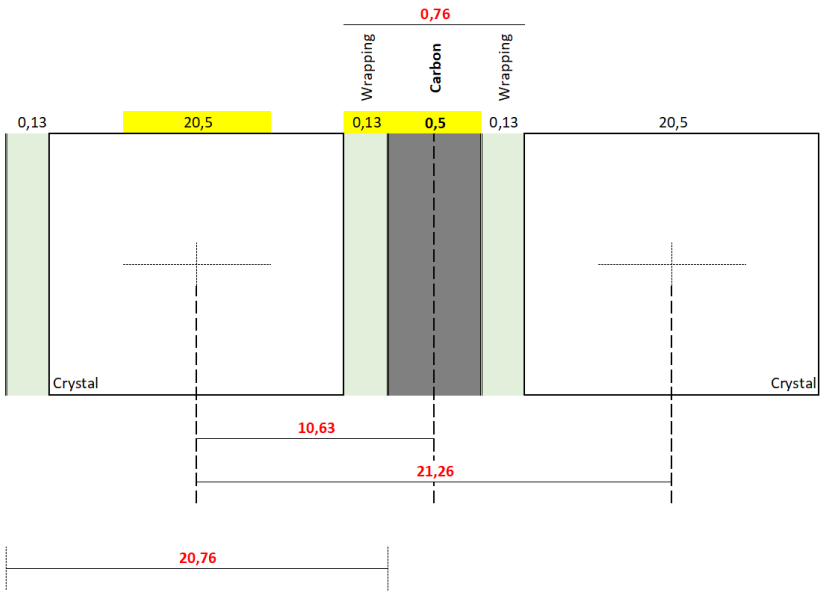

Figure 8: Space between crystals in mm (not to scale)

The drawing in Figure 8 gives an example of the positioning of the crystals, the wrapping, and the carbon plate.

2.5 Configuration of the crystals

2.5.1 Selected solution for the detailed design

The solution consists in positioning the center of the detector so that it passes through the center of a crystal as described in Figure 9. The arrangement of the crystals is clearly optimized when both the horizontal and vertical axes pass through the center of a crystal. In addition, the mechanical structure can be symmetric with this configuration of crystals. All the crystals are stacked with a 0.5 mm (at most) carbon plate separating each of them. This ensures precise alignment while providing mechanical stability and structural integrity to the assembly.

- All the configurations were tested with $t = 0.5$ mm and $D = 1306$ mm
- Total number of crystals = 2722 (without optimization near the beam pipe)
- The centered solution has the advantage of making the mechanical structure symmetrical.

2.5.2 Beam-pipe area

The main objective is to be as close as possible to the beam pipe. We can add crystals in the corners as shown in Figure 10. We can explore different designs for the internal structure, either rectangular or following the shape of the beam-pipe flange. Regarding the thermal aspects, both mechanical designs could have the same capabilities.

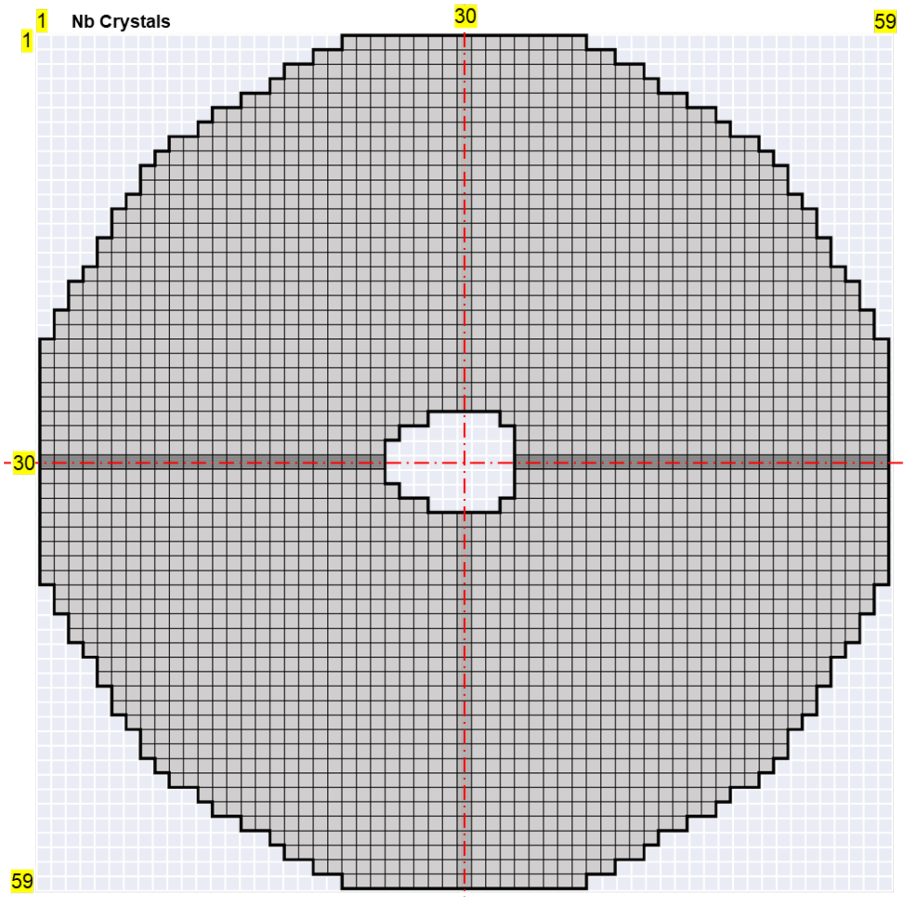

Figure 9: Configuration of the crystals

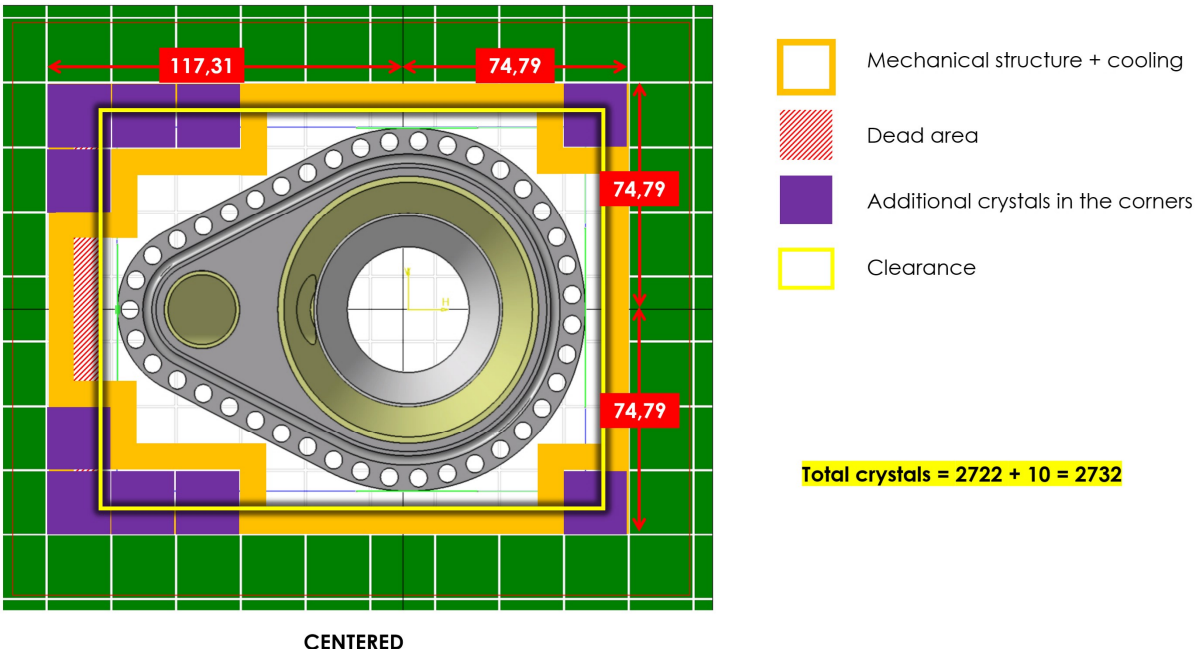

Figure 10: Conceptual design. Drawing to estimate the additional crystals near to the beam pipe. Configuration of the crystals around the beam pipe for the centered configuration.

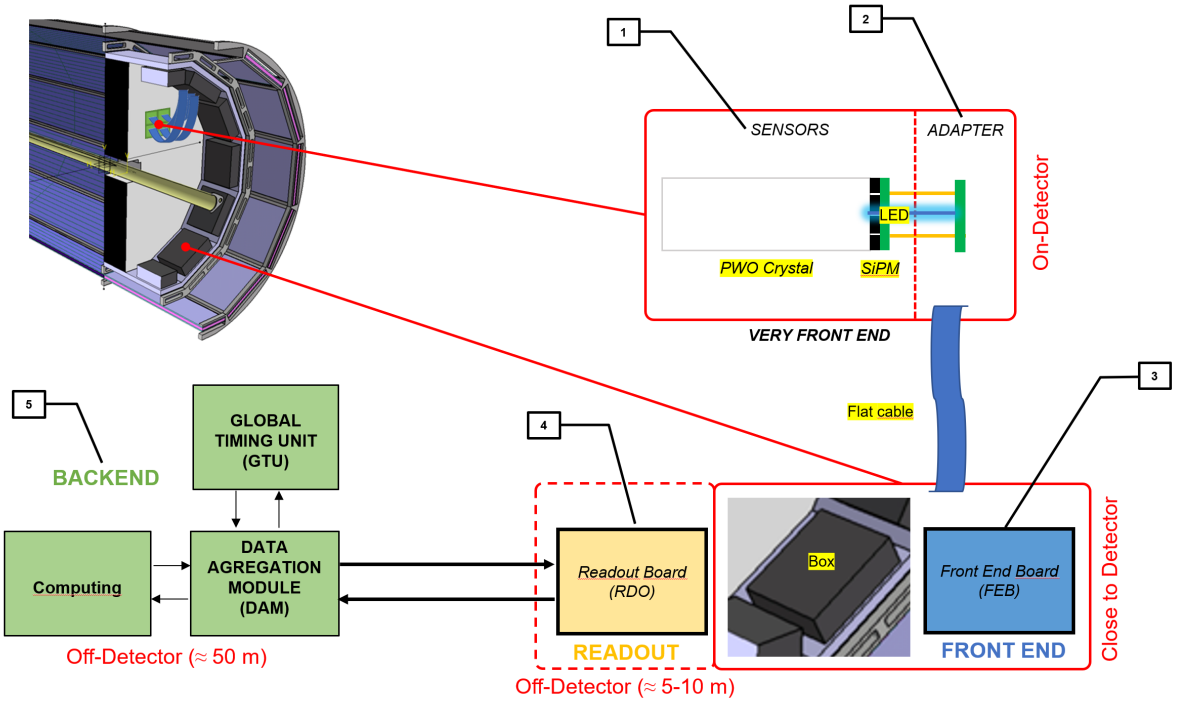

Figure 11: Overview of the DAQ and the main components of the readout

Table 3: Main components of the DAQ

n°	Designation	Description
1	SENSORS	SiPM
2	ADAPTER	PCB SiPM
3	Front End Board (FEB)	ASIC or Discrete
4	Readout Board (RDO)	FPGA
5	BACKEND	GTU, DAM, Computing

3 Readout setup

3.1 DAQ overview

It is necessary to briefly describe the Data Acquisition System (Figure 11) to identify where the main sources of power dissipation are located. This overview will also highlight the necessary cables and provide a designation of the components (Table 3) involved in the readout system.

The stability of the crystals temperature is one of the most critical requirements for physics performance. The main objective is to position the Front End Board (FEB) as far away as possible from the crystals. This is crucial because the power consumption, primarily concentrated in the FEB, could significantly impact the temperature stability of the crystals. The very front end, consisting of a SiPM PCB and an adapter PCB (described in the following sections), can be placed closer to the crystals. The effects of radiation on SiPMs are slow and progressive, and we estimate a power consumption increase of 0 to 10 W over one year for the full detector due to SiPM irradiation, based on experience from the STAR detector. This aspect is further detailed in section 4. The Readout Board (RDO) should not be placed close to the detector. There is an advantage to positioning the RDO 5 or 10 meters away, as its power consumption is

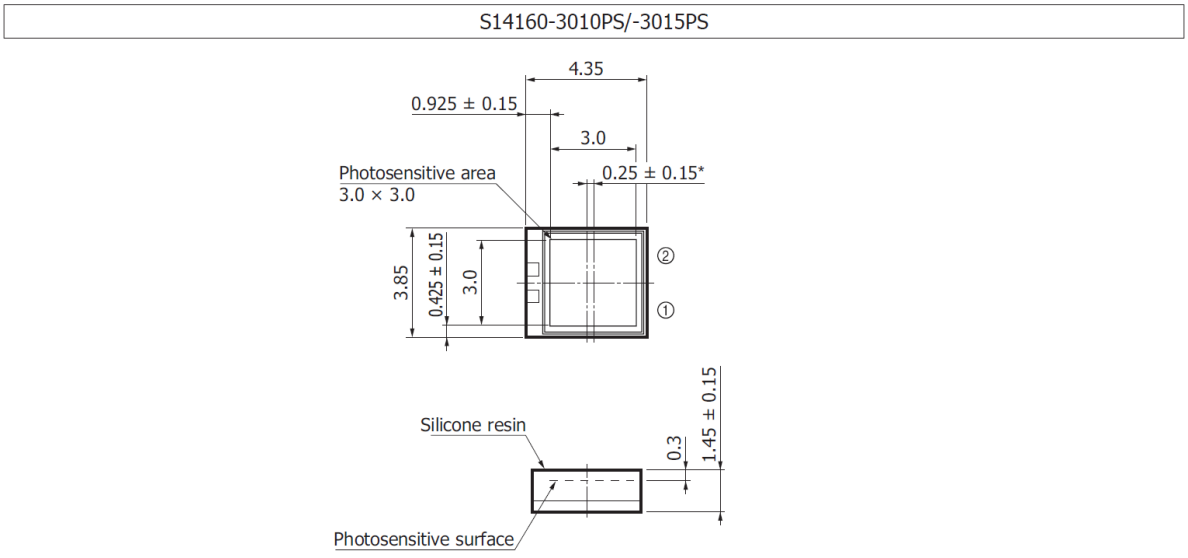

Figure 12: Dimensions of the SiPM Hamamatsu S14160-3015PS

a	Transverse x size of the crystal	20,5 *mm*		Surface crystal	420,25 *mm2*	
	Matrix crystals	1 *x* 1		Surface SiPM	16,75 *mm2*	
d	Space between crystals (carbon+wrapping)	0,76 *mm*		Detection active SiPM	3,00 *mm*	
	Transverse y size of the crystal	20,5 *mm*		Surface active SiPM	9,00 *mm2*	
				Total active SiPM	144,00 *mm2*	
h	SiPM	4,35 *mm*		Active surface SiPM	34,27 *%*	
l	SiPM	3,85 *mm*		Distance SiPM / Cristal	H	1,250 *mm*
h x l	Matrix SiPM	4 *x* 4		Distance SiPM / Cristal	L	2,250 *mm*
e	Space between SiPM	0,2 *mm*				
H	Matrix SiPM	18 *mm*				
L	Matrix SiPM	16 *mm*				

Figure 13: Surface area covered by the SiPMs

several dozen watts. If placed within the cooled boxes behind the crystals, the cooling system would need to be sized accordingly to dissipate this additional heat. The positioning of the power supplies depends on the design of the FEB.

3.2 SiPM configuration

The description of the SiPM configuration is based on Hamamatsu S14160-3015PS, and its dimensions are provided in the Figure 12. The mechanical solution for fastening the very front-end is dependent on the SiPM size: 3×3 mm^2 or 6×6 mm^2.

The SiPM configuration is based on a 4×4 layout, consisting of 16 SiPMs. It was not possible to add additional SiPMs to cover more of the crystal surface because mechanical clearance is required to fasten the very front-end to a grid. The fastening of the very front-end is described section 6. The effective surface area covered by the SiPMs is about 34%, as explained in Figure 13.

The current configuration uses an LED on the SiPM board for gain monitoring. The LED is

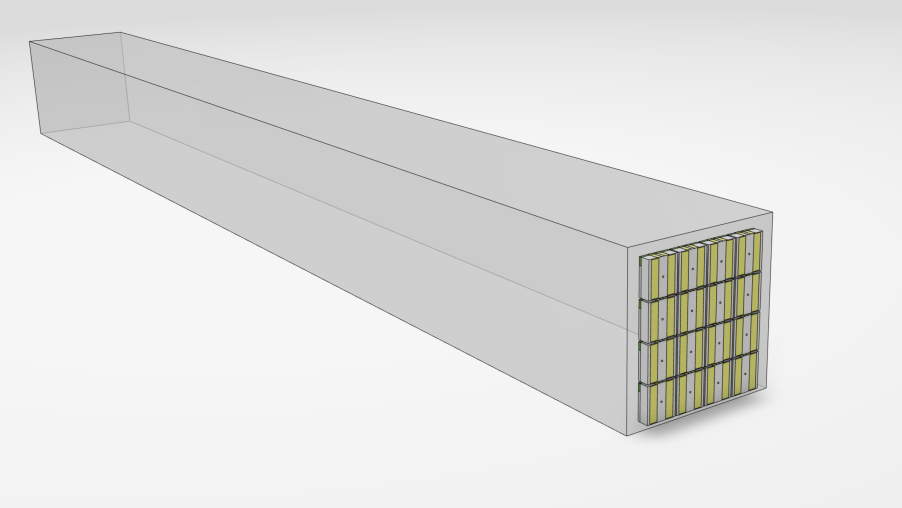

Figure 14: Positioning of the SiPMs on the crystals, not perfectly centered

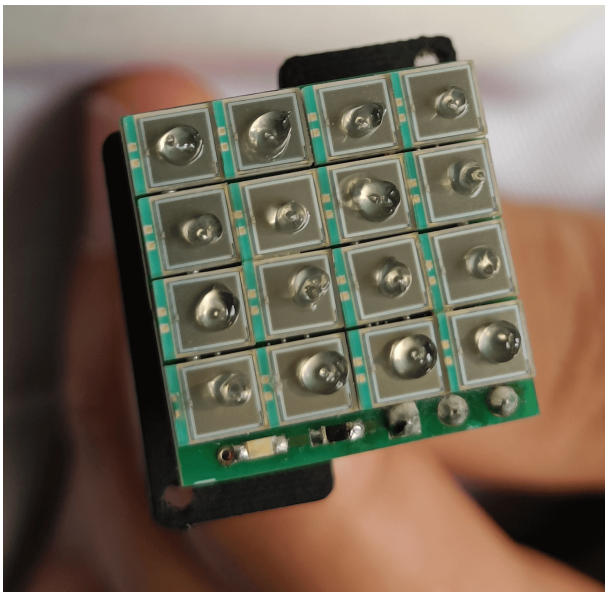

Figure 15: Small drop of optical grease on each SiPM

positioned at the edge of the PCB, which explains why the 16 SiPMs are not perfectly centered on the crystals (Figure 14). An alternative solution could be to place the LED in the middle of the PCB. The details of the SiPM PCB are given in section 3.3.

3.3 Very front end

The Very Front End (VFE) of the detector system is a critical interface that ensures efficient signal acquisition and transmission. It consists of two main components: the SiPM PCB and the adapter PCB. SiPMs are optically coupled (Figure 15) to the PWO crystals, ensuring optimal light collection from the scintillation process. The SiPM PCB handles the direct signal capture from the SiPMs, while the adapter PCB facilitates the connection to subsequent electronics, enabling transmission of the signals for further processing (Figure 16).

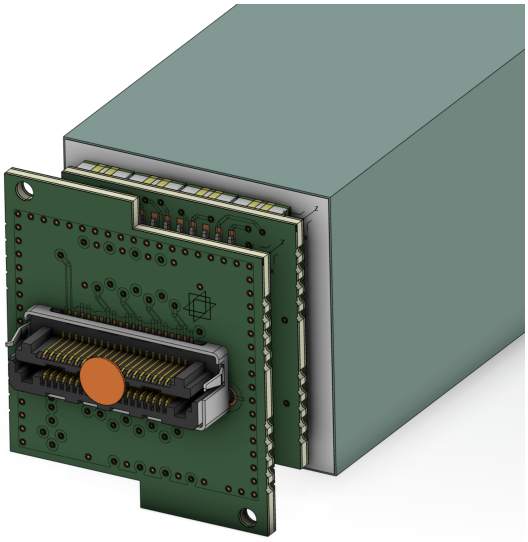

Figure 16: Very Front End with SiPM & adapter PCBs

3.4 Readout options

The readout configuration has not been defined yet, but three possible options are currently under consideration, as summarized in Figure 17. The first option consists of reading all signals of a crystal in parallel, providing a simplified approach but potentially reducing individual signal performance. The second option involves merging signals in groups of four, offering a balance between complexity and data granularity. Finally, the third option would read each SiPM individually. The final choice will depend on the trade-off between signal resolution, complexity, and overall system performance. The beam test results will be crucial in determining the most suitable readout configuration. Evaluating the performance of each option under real experimental conditions will provide key insights into signal quality, noise levels, and overall system performance.

3.5 5×5 prototype

In order to test and validate some technical aspects, a prototype with 25 crystals has been built (5×5 prototype). In this section, a schematic drawing of the setup used for the DAQ is provided for information (Figure 18). The mechanical design of the prototype is described in section 4.6.

4 Cooling

4.1 Specifications

To ensure the physics requirements in terms of temperature stability, it is necessary to cool the crystals to maintain a stability of ±0.1 °C (standard deviation). Temperature stability is critical for long-term operation and must be carefully verified. The closeout report from the 2022 EIC Project detector technical review of the electromagnetic and hadronic calorimetry [8] highlights that a temperature variance of 0.5 °C already results in a 1.2 % change in light yield, which directly affects the constant term of the energy resolution. The reviewers emphasized that the stability could be compromised by the proximity of the front-end electronics. As discussed in section 3, the solution to mitigate this effect is to position the power sources as far as possible from the crystals. Another comment from the review focused on the long stabilization time due

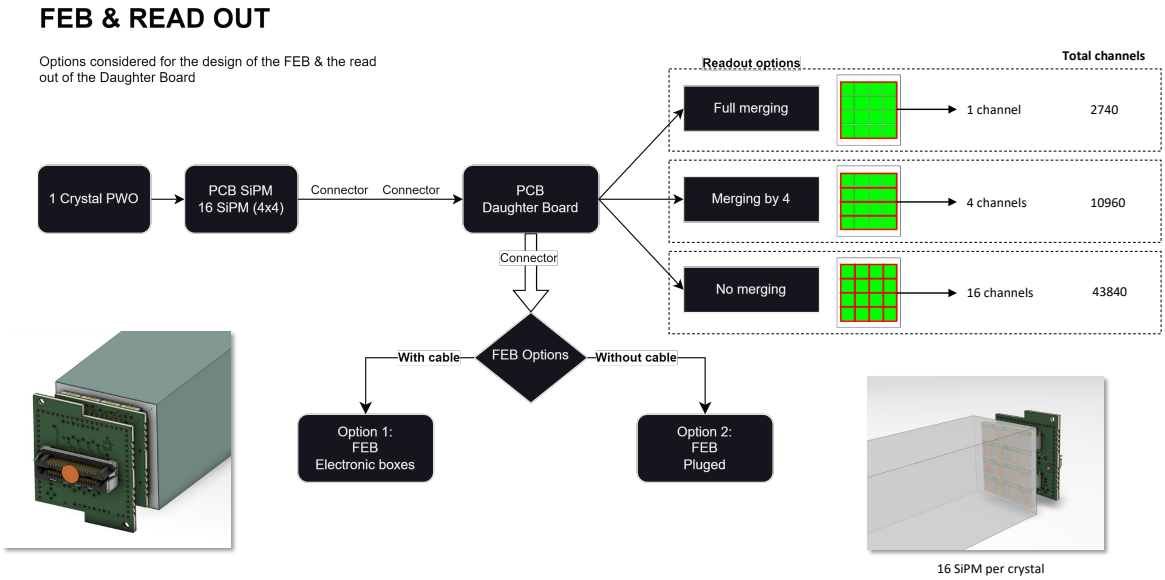

Figure 17: Different options considered

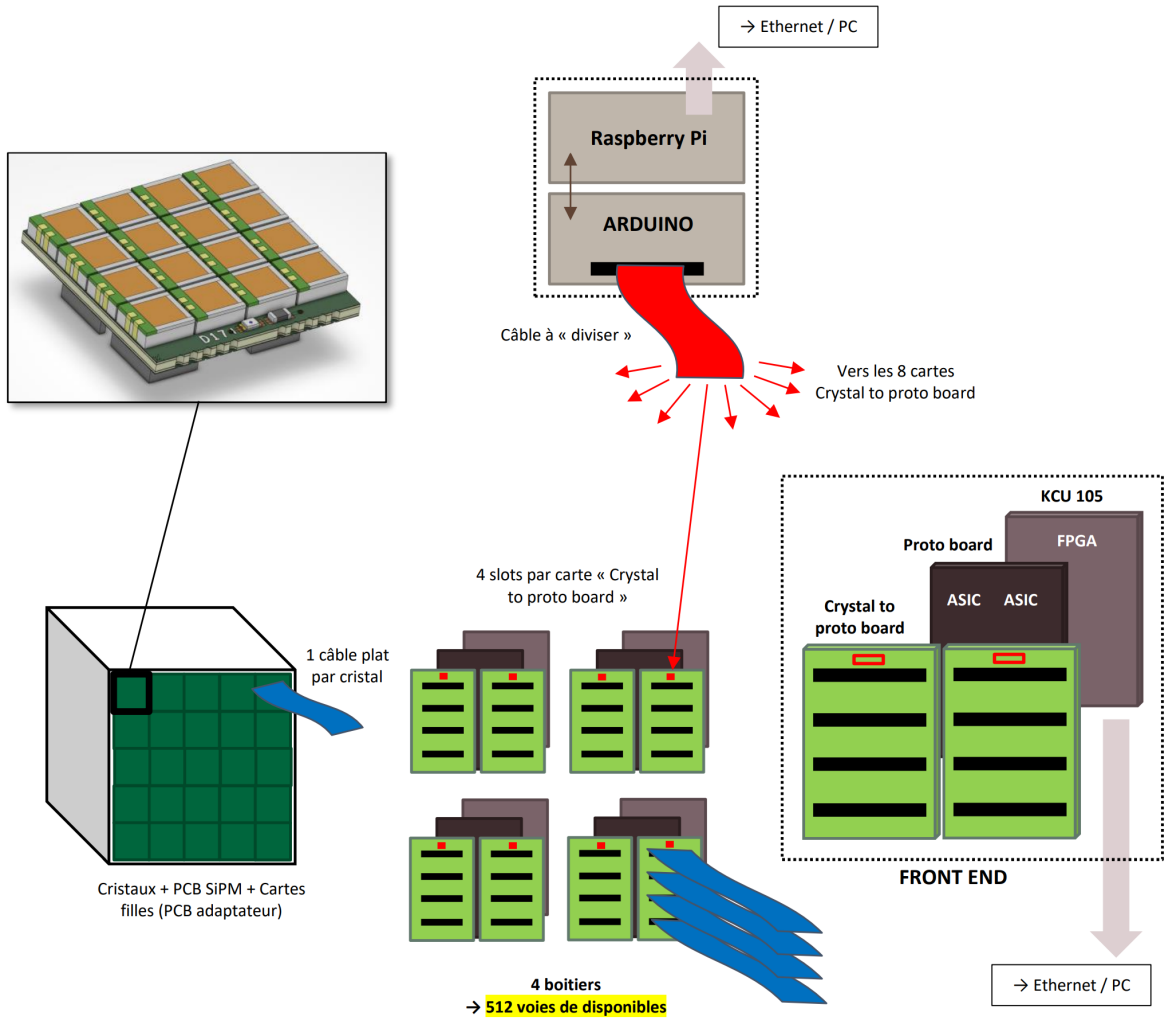

Figure 18: DAQ setup used with the prototype 5×5 for the beam tests @CERN & @DESY performed in 2024 and 2025

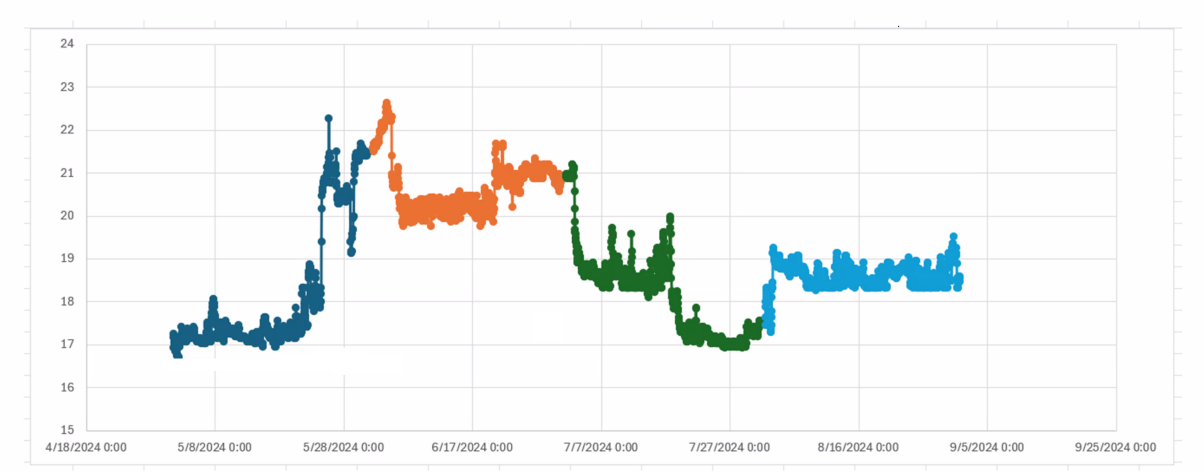

Figure 19: Stability of the temperature to be considered for the design of the cooling (±1.5 °C)

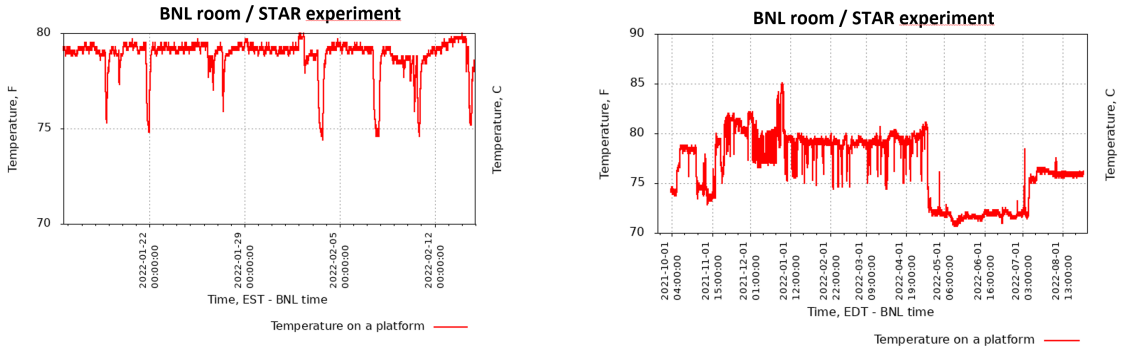

Figure 20: Temperature stability in BNL experimental hall

to the low thermal conductivity of PWO. It was noted that whether the crystals are operated at room temperature (CERN) or at -25°C (PANDA), the main issue remains the temperature stability. In our case, the primary design consideration is the stability of the experimental room temperature, which is expected to vary by about 3°C. This estimation is based on observed temperature fluctuations in the RHIC experimental area, as shown in the orange region in Figure 19, and Figure 20.

Regarding the potential impact on the stability of the nearby pfRICH subdetector (Figure 21), the heat generated will be managed by a cooling system, and the surrounding temperature is expected to remain close to the ambient level.

The sizing of the system depends on three main parameters. First, the amplitude of the temperature variations in the experimental hall, which determines the extent of thermal expansion and contraction that the system must accommodate. Second, the frequency or period of these temperature variations, as rapid fluctuations may require a more responsive thermal management strategy. Finally, the location of the power dissipation plays a crucial role, as it influences heat distribution and the efficiency of cooling solutions. These factors must be carefully considered to ensure the stability and performance of the system.

- The amplitude of the temperature variations in the experimental hall $\rightarrow \Delta T = 3°\mathbf{C}$

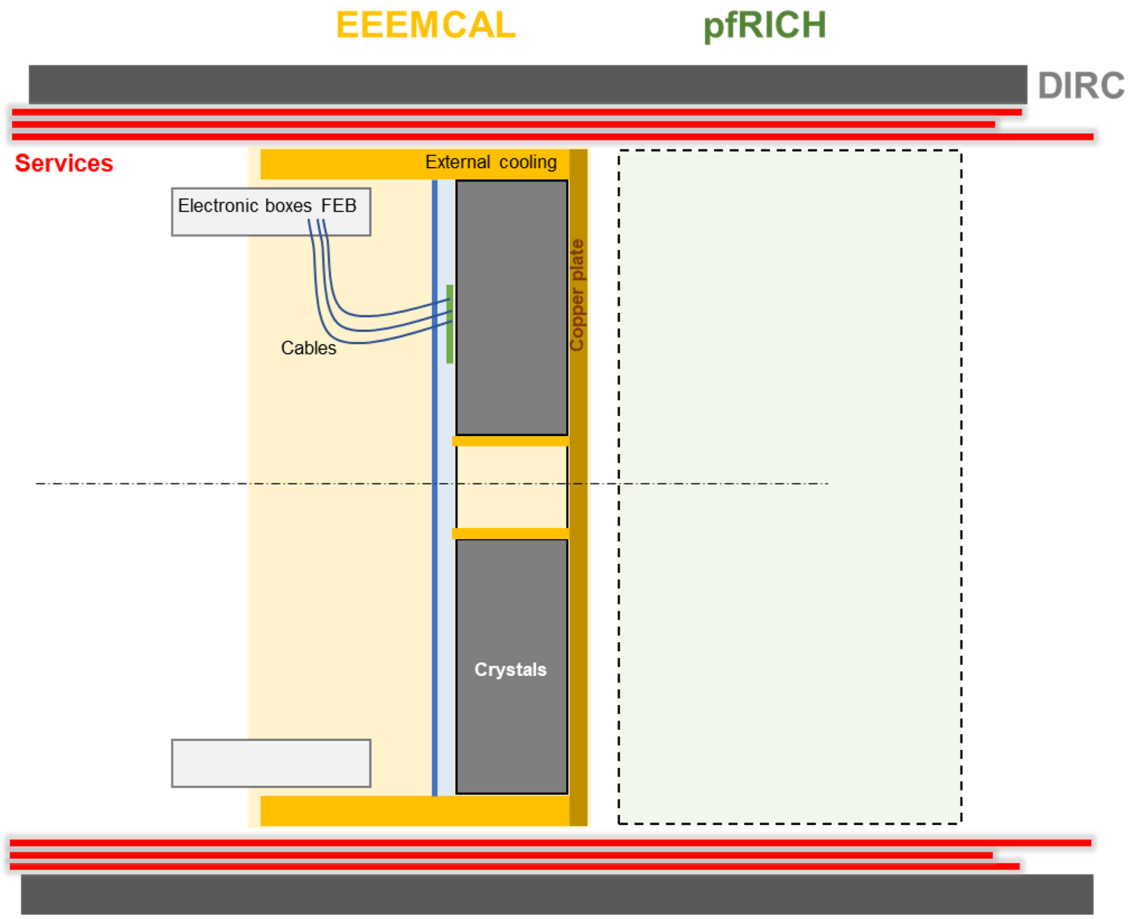

Figure 21: Positioning of the EEEMCal with respect to the pfRICH

- The frequency/period of the temperature variations in the experimental hall → **6 hours < T < 12 hours**
- The location of the power to dissipate → **Power on electronic boxes**

4.2 Description of the cooling system

The cooling system is divided into two main sections: the first one focuses on cooling the crystals, and the second one on cooling the electronic boxes housing the Front-End Boards (FEB). To stabilize the crystals, the cooling can only be applied around the outer diameter, around the inner beam tube hole, and at the front of the detector. The rear side, where the very front-end is located, presents significant challenges for cooling. However, fastening the components onto an aluminum grid may provide some cooling through thermal conductivity with the internal and external cooling systems. For the electronic boxes, with each box dissipating approximately 100 W (assuming 12 boxes), two cooling options are being considered: one using cold plates, and another one using heat exchangers and fans. Figure 22 describes the solutions for the cooling system.

The cooling of the electronics is a critical aspect currently under study, with several options being considered based on the design of the Front-End Boards (FEB) and the readout system. The first option involves placing electronic boxes around the calorimeter along the external diameter, ensuring uniform cooling but requiring efficient heat dissipation management. The second option positions the boxes in front of the SiPMs, with two possible configurations: using cables, which necessitates cooling via fans and heat exchangers, or a direct-contact solution where a cold plate cools the FEBs plugged onto the SiPM. The third approach consists in mounting the FEBs on racks distributed around the external diameter of the EEEMCal, which could offer modularity but requires an optimized thermal strategy. The three solutions are summarized in Figure 23. The beam tests and further simulations will help determine the most effective solution for maintaining temperature stability while ensuring optimal performance of the readout electronics.

One of the key parameters for sizing the chillers required for cooling is the pressure drop. This aspect is further detailed in next sections, where the relationship between the cooling system design and the pressure variations is discussed. Properly managing the pressure drop is essential to ensure efficient cooling and stable operation of the system.

4.3 Cooling of the crystals

4.3.1 Design for the simulation

To evaluate the impact of temperature variations in the room, several cases were tested to assess the efficiency of each component. One key objective was to verify the effectiveness of the insulation in maintaining stable thermal conditions. Additionally, particular attention was given to ensuring that no power sources were placed near the crystals, minimizing potential thermal disturbances.

The simplified design and the main parameters for the simulations are described in Figure 24.

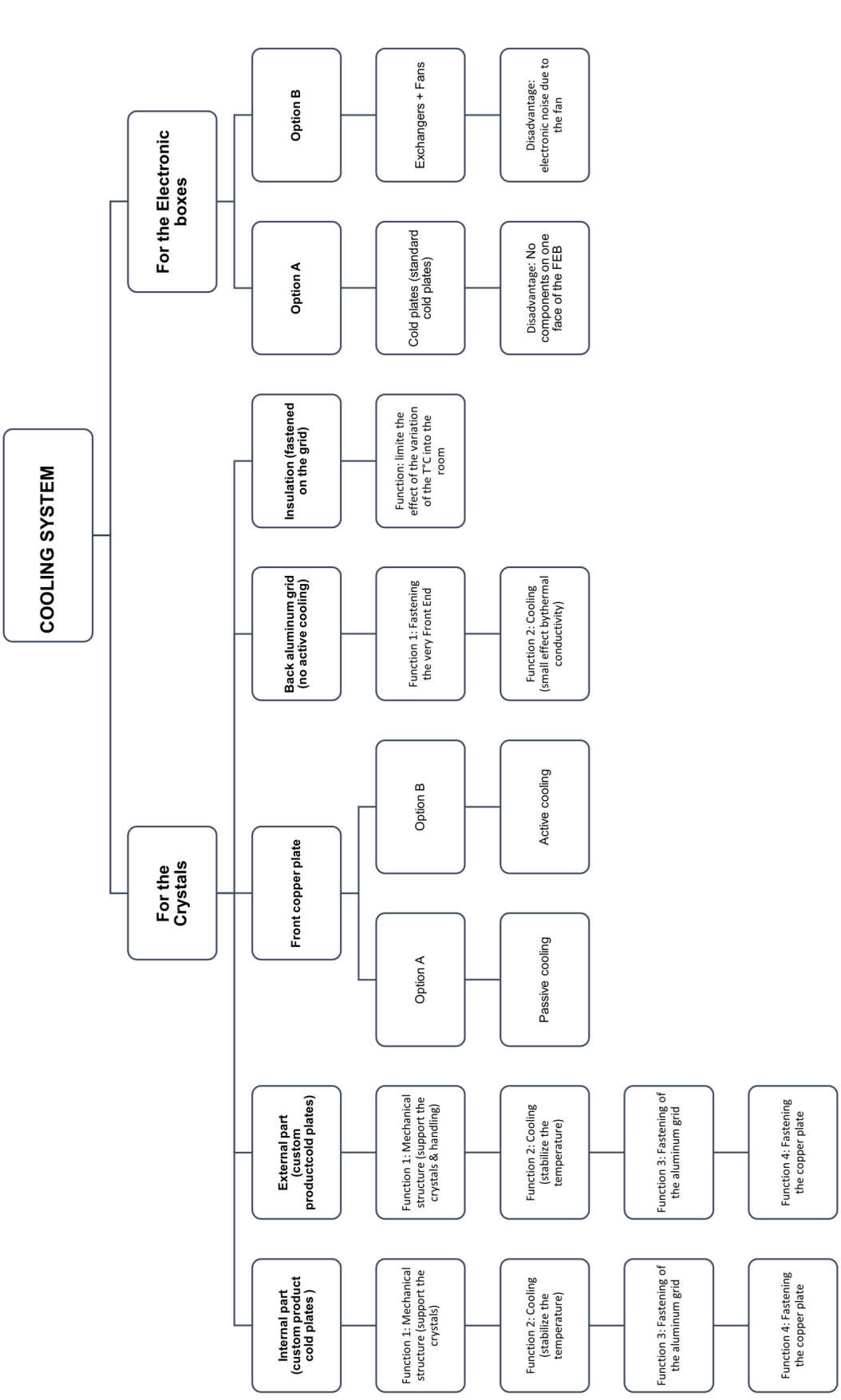

Figure 22: Description of the cooling system

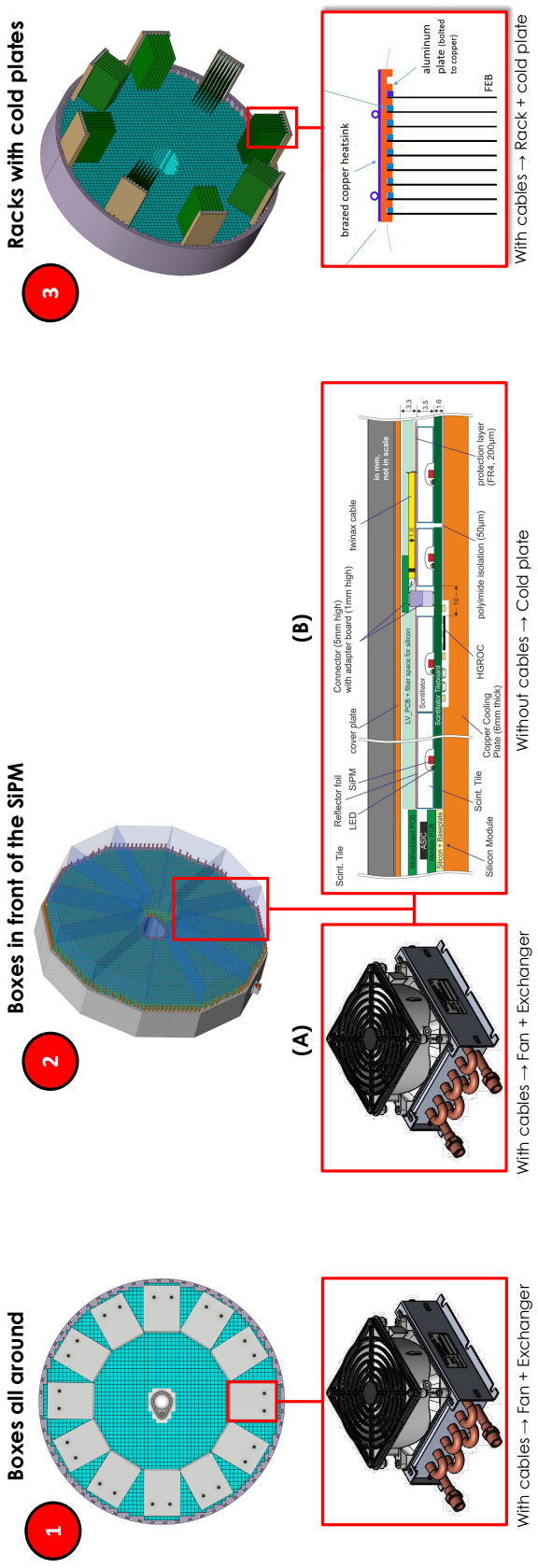

Figure 23: Options considered for the cooling of the electronics

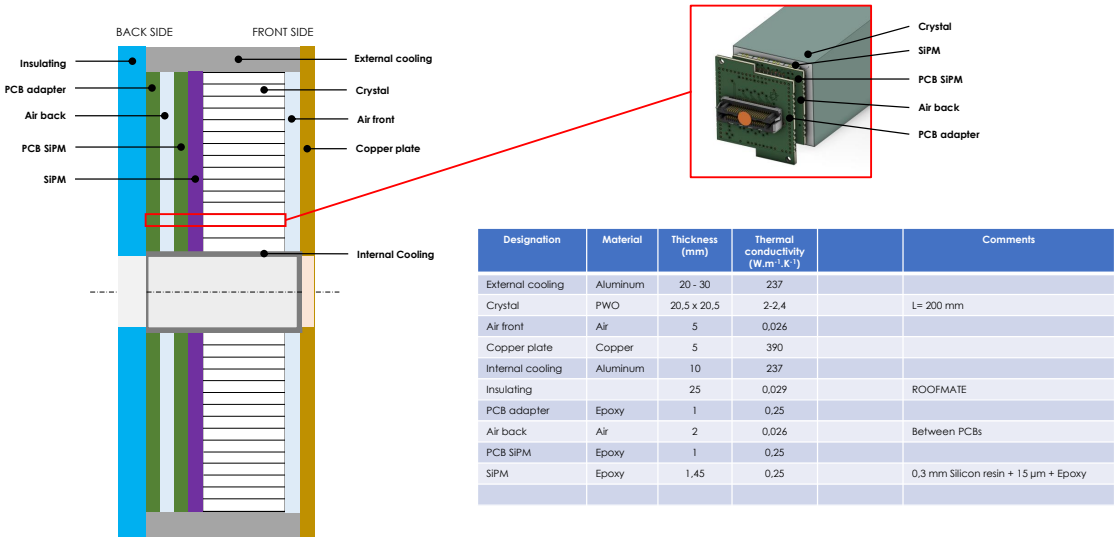

Designation	Material	Thickness (mm)	Thermal conductivity ($W.m^{-1}.K^{-1}$)		Comments
External cooling	Aluminum	20 - 30	237		
Crystal	PWO	20,5 x 20,5	2-2,4		L= 200 mm
Air front	Air	5	0,026		
Copper plate	Copper	5	390		
Internal cooling	Aluminum	10	237		
Insulating		25	0,029		ROOFMATE
PCB adapter	Epoxy	1	0,25		
Air back	Air	2	0,026		Between PCBs
PCB SiPM	Epoxy	1	0,25		
SiPM	Epoxy	1,45	0,25		0,3 mm Silicon resin + 15 µm + Epoxy

Figure 24: Overview and main parameters for the ANSYS simulations

4.3.2 ANSYS simulation: steady state

Both external and internal cooling are assumed to be at the same temperature of 19°C. Additionally, a low-temperature gradient along the crystal is maintained, ensuring that $\Delta T = 2°C$. Figure 25 gives an example of the results for a particular case.

A thermal model was developed to evaluate the impact of room temperature variations on system stability. Two steady-state simulations were conducted: the first one with a room temperature of 23°C and the second one with a room temperature of 26°C, representing a worst-case scenario for comparison. The results indicate that without insulation, the temperature variation reached 1.6°C, whereas with insulation – consisting of foam, air, and copper – the stability improved significantly, reducing ΔT to just 0.4°C. This demonstrates the effectiveness of the insulation in mitigating thermal fluctuations. Figure 26 shows the comparison between two steady states.

Results for the stability:

- Without insulation : $\Delta T = 1{,}6°C$
- With insulation (foam, air and copper) : $\Delta T = 0.4°C$

4.3.3 ANSYS simulation: transient state

A transient thermal model was developed to analyze the system response to a room temperature decrease from 26°C to 23°C over a period of 6 hours, with a total cycle duration of 12 hours. The simulation started from a steady-state condition at 26°C. The results indicate excellent thermal stability, as we can see in Figure 27, with temperature variations (ΔT) remaining below 0.1°C.

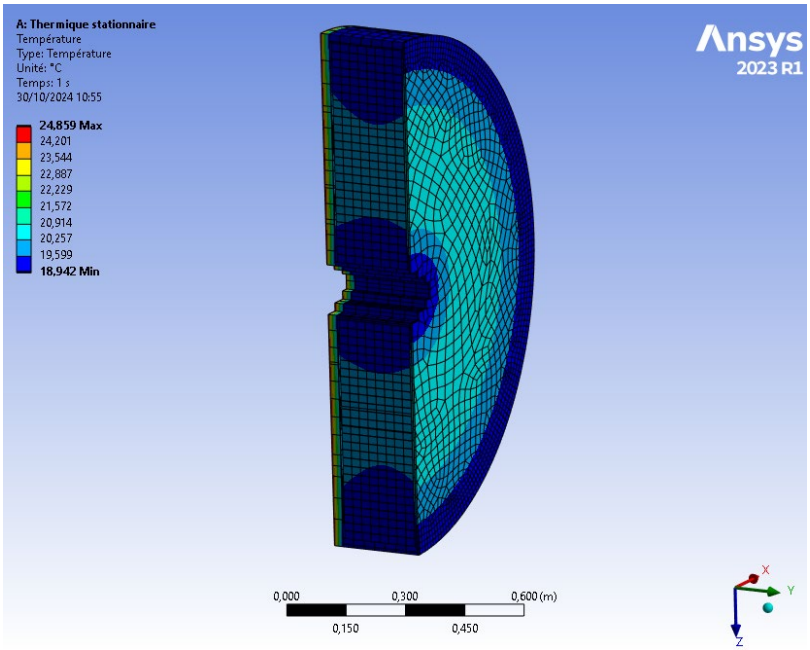

Figure 25: Steady state ANSYS simulation: distribution of the temperature on the crystals with a room temperature at 26°C and a cooling temperature at 19°C

Additionally, due to the thermal inertia of the crystals, there is a delay between the moment when the room temperature starts to rise again and the moment when the temperature of the crystals begins to increase. This shift, caused by the time required for heat to transfer and stabilize within the material, is estimated to be between 1 and 2 hours. These findings are consistent with data from the NPS experiment [9].

4.3.4 ANSYS simulation: effect of SiPM radiation damage

The effect of radiation on the SiPMs results in an increase in dark current and power dissipation. Based on experience in STAR, we estimate a power dissipation of approximately 10 W for the entire detector (corresponding to 3.54 mW per crystal on average) after 1 year of irradiation. This additional power input leads to a significant temperature rise, ranging between 0.4°C and 0.8°C. However, the radiation damage of SiPM will be slow compared to the temperature variations of crystals, and therefore the temperature stability remains unaffected. The temperatures for the crystals at the bottom of the detector are compared in Figure 28 with and without this extra source of heat (gradual increase up to 3.54 mW over 1 year).

4.4 Cooling for the electronic boxes, Front End Board (FEB)

As described in section 3.1, the solution to ensure the stability of the crystal temperature is to relocate the power source to electronic boxes all around the external diameter of the EEEMCal. In the configuration with 12 boxes, the power to dissipate is approximately 120 W per box. It is easier to cool each box independently than to develop a cooling system close to the crystals. The estimated power consumption is 0.15 mW per channel, plus an additional 0.15 mW for other components.

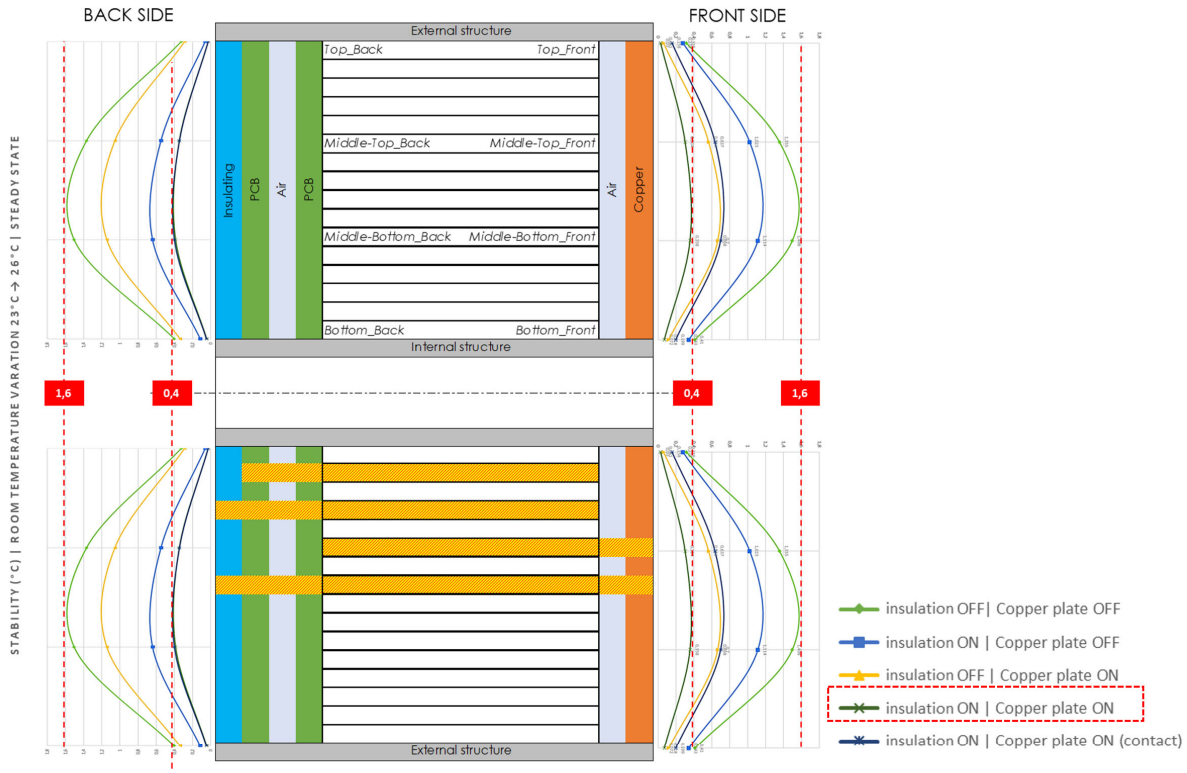

Figure 26: Two steady states comparison: with and without insulation. Curves show the temperature difference at the front and back of the crystals when a steady-state simulation is performed at 23°C room temperature, and another steady-state simulation is performed at 26°C room temperature. The temperature difference is small for crystals close to either the internal or external cooling structures but increases for crystals away from them. Without insulation or a copper plate in front of the crystals (green curves), this difference reaches 1.6°C. With insulation and a copper plate in front of the crystals, this difference is reduced to a maximum value of 0.4°C (black curves).

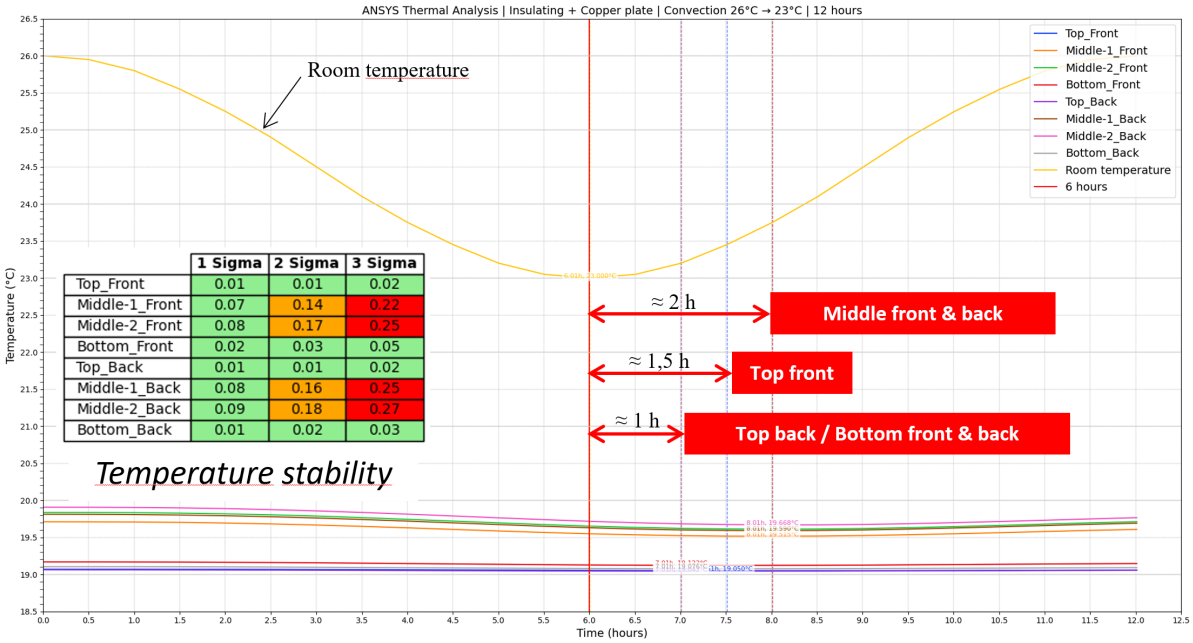

Figure 27: Evolution of the crystal temperatures for a variation of the room temperature from 26°C to 23°C in 6 hours and from 23°C to 26°C in 6 hours. The red arrows indicate the time lag between the moment when the room temperature begins to rise again and the moment when the temperature of the crystals starts increasing.

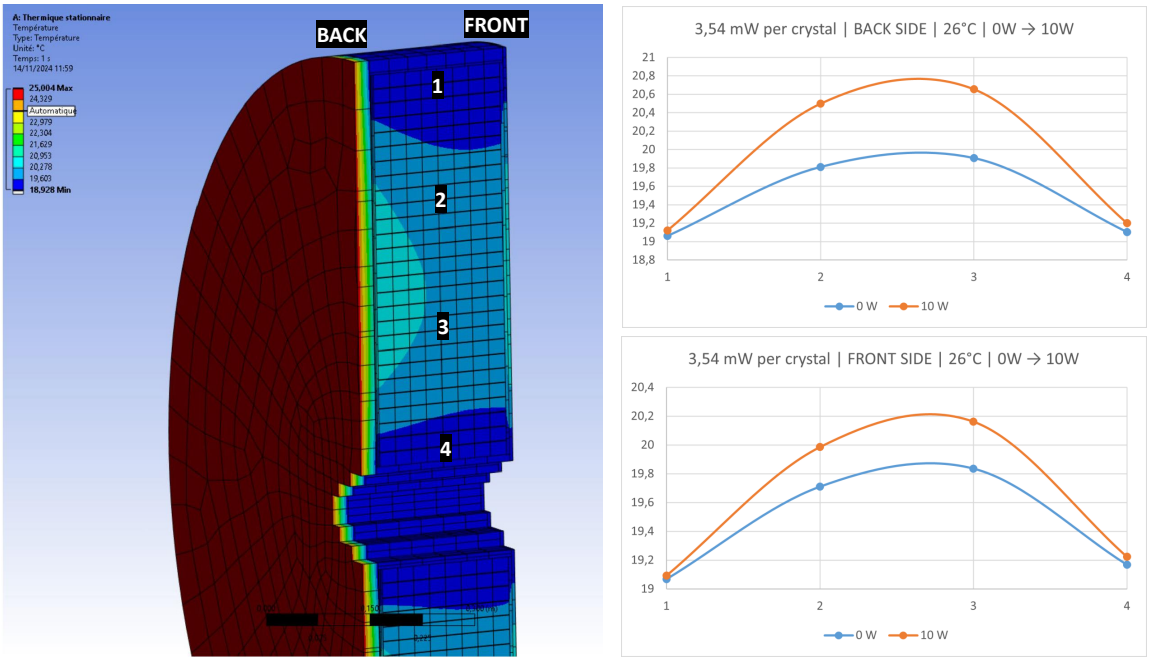

Figure 28: Steady state simulation: room temperature is 26°C and cooling is at 19°C. The right plots show the temperature variation at the front and back of a crystal, with and without a 10 W additional power source in the detector (3.54 mW in a crystal).

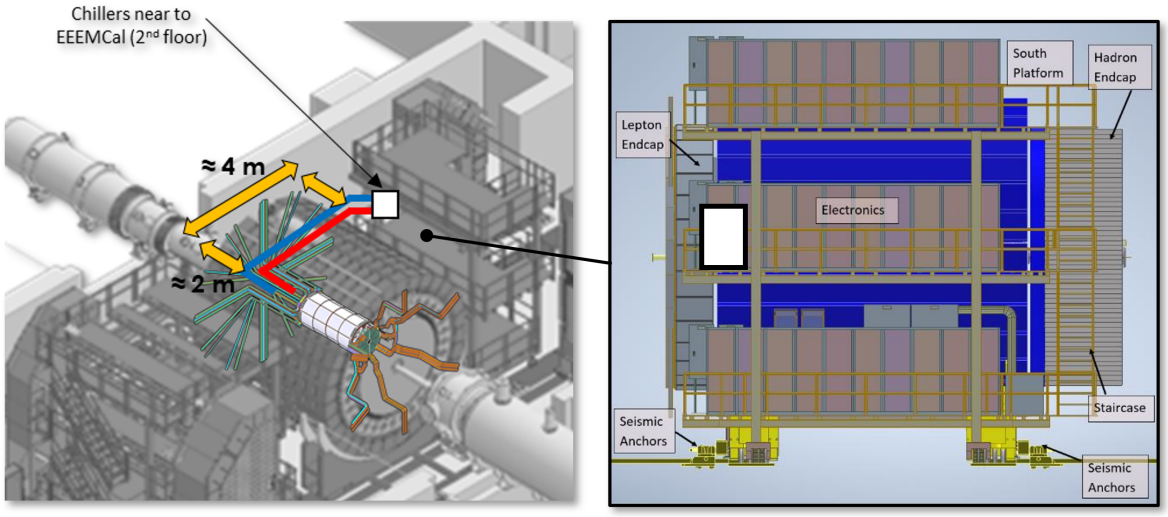

Figure 29: Location of the detector chillers, indicated by the white rectangle in the left and right figures.

30 mW by channel & (3000 crystals x 16 SiPMs)/(12 boxes) → 120 W/box

4.5 Chillers and pressure drop

When analyzing pressure losses in the cooling system, several key factors must be considered. The location of the chillers plays a crucial role in determining the overall efficiency of heat dissipation and fluid circulation. Additionally, the entire network of cooling tubes must be carefully designed to minimize resistance and ensure an optimal flow rate. Finally, the power of the chiller pump is a critical parameter, as it must be sufficient to compensate for pressure drops across the system while maintaining stable and efficient cooling performance. As discussed with the 3I Team and the chief engineer, the chillers can be placed close to the detector on the same plane (see Figure 29). This positioning significantly reduces gravitational losses, ensuring a more efficient and stable cooling system.

The pressure drop in the cooling system also depends on the roughness of the internal surfaces of the tubing. Variations in surface finish can impact fluid resistance, potentially altering the overall efficiency of the system. Additionally, the results may vary depending on the construction method used for the external structure, which can influence the layout and connections of the cooling network. The first-order analytical calculations indicate very encouraging results (Figure 30). Once the design is further consolidated, a more detailed analysis will be conducted using ANSYS and Fluent to validate the initial findings. These simulations will help refine the thermal and mechanical performance, ensuring the proposed solution meets the required specifications.

4.6 5×5 prototype

To conduct instrumental tests, a prototype consisting of 25 crystals (5×5 matrix) was constructed. The testing phase included placing the prototype in beamlines, with one test conducted at CERN from August 28 to September 12 (2024), and another one at DESY from February 17 to March 2 (2025). The prototype features four cold plates surrounding the crystals and a 5-mm-thick copper plate in the front face. Additionally, an aluminum grid is used to fasten the very front-end electronics. Several thermal tests were performed, first in an un-

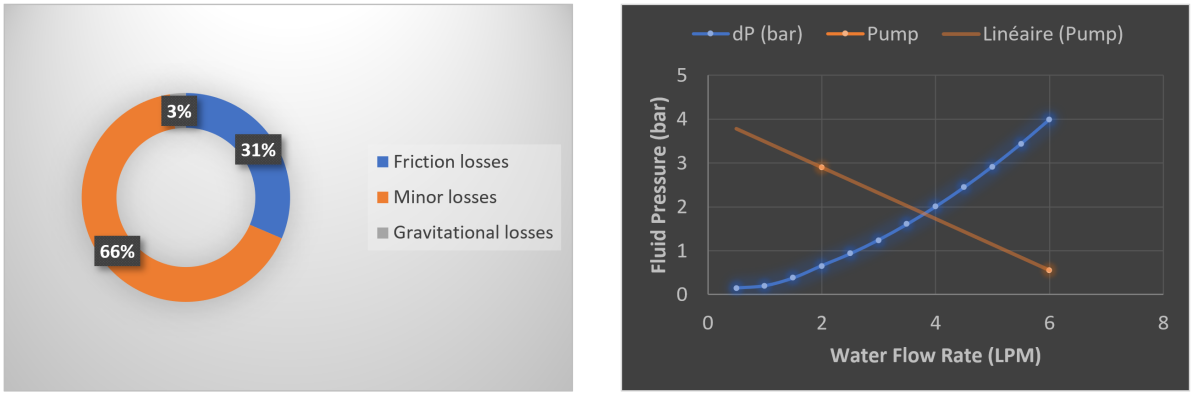

Figure 30: Most of the pressure drop come from minor losses. The length and shape of the cooling system could be optimized to reduce these losses. The right plot demonstrates that the cooling system functions effectively and compensates for the pressure drop with the operating point around 2 bar.

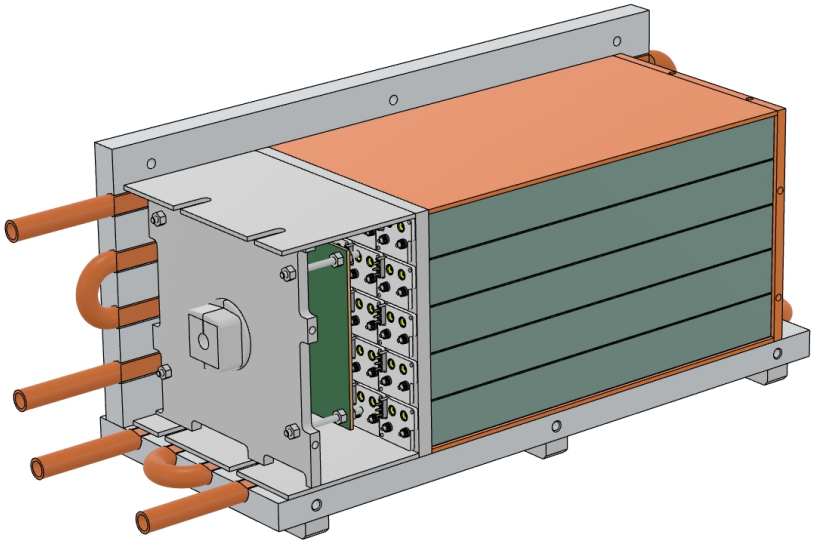

Figure 31: Overview of the prototype 5×5

controlled temperature environment and later during the beam tests. However, the prototype is not entirely representative of the final EEEMCal detector. In the prototype, the four cold plates are separated by only five crystals, creating favorable cooling conditions. In contrast, in the final EEEMCal detector, the distance between the internal and external cooling systems is approximately 500 mm, compared to around 100 mm in the prototype, making the performance results less applicable to the larger scale setup.

4.6.1 Mechanical design

The CAD design of the 5×5 prototype is shown in Figure 31.

To reduce costs, the mechanical design is based on four standard cold plates (Figure 32), with their performance detailed in the accompanying Figure 33. One of the primary objectives of this thermal prototype is to confirm the necessity of distancing the power sources from the

Figure #2

- #120456 & #120457

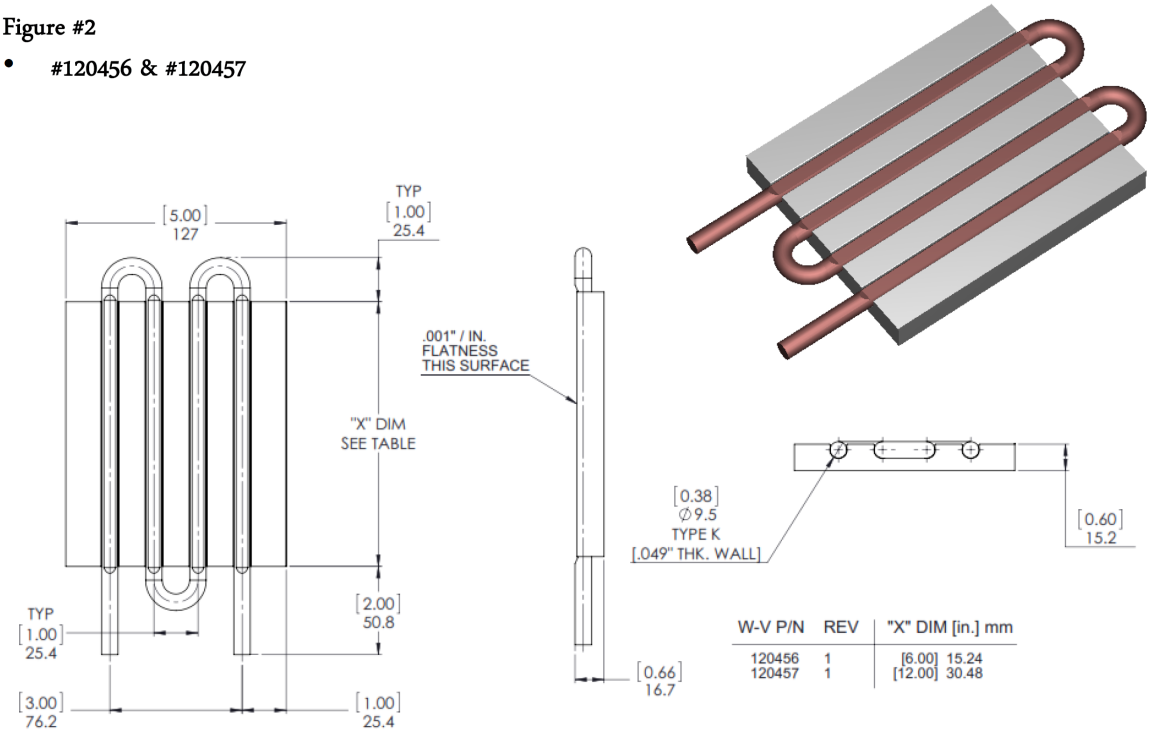

Figure 32: Drawing of the cold plates used for the 5×5 prototype

crystals. To test this hypothesis, a PCB with resistors was created to simulate the power consumption of the front-end electronics. This PCB was positioned in front of the aluminum grid, approximately 30 mm from the crystals.

The initial phase of thermal tests, conducted without the actual crystals and without the very Front End (SiPM and Adapter PCBs), used "fake" crystals made of natural stone (Figure 34). The thermal conductivity of this stone is comparable to that of PWO, approximately 3 W/mK, ensuring the measurements closely mimic the real thermal conditions expected in the final setup. In addition, it is a very cheap solution.

4.6.2 Thermal test without cooling

The first test was conducted without cooling, the main objective being to adjust the setup and quantify the effect of room temperature on the system. This initial phase allowed for the identification of potential thermal variations and provided a baseline for comparison when the cooling system was implemented. The second objective was to simulate a power source positioned in front of the crystals (Figure 35).

This test aimed to evaluate the impact of localized heating on the system and assess how thermal variations could affect the detector performance. The results (Figure 36 and Figure 37) will help to optimize the cooling strategy and to ensure temperature stability during operation.

Temperature stability with power in front of the crystals and without cooling → ±0.5 °C

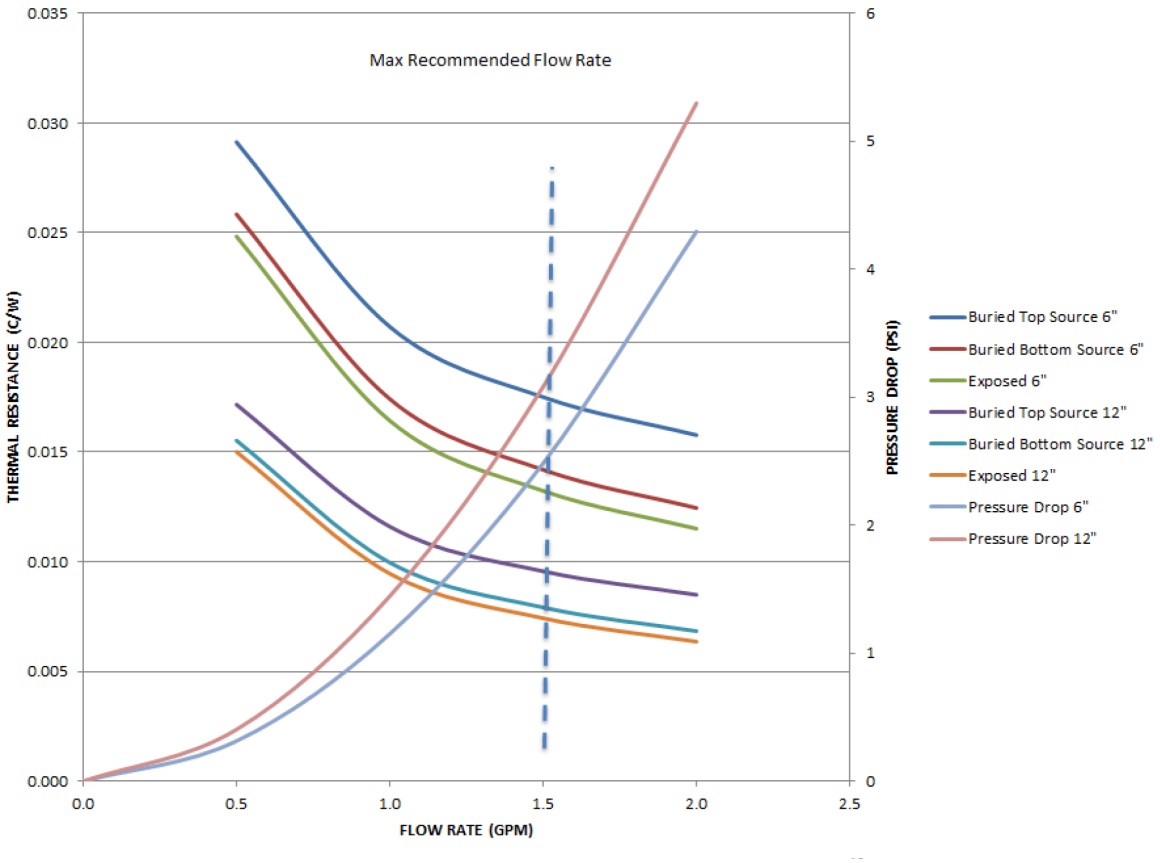

Figure 33: Datasheet describing the performances of the cold plates

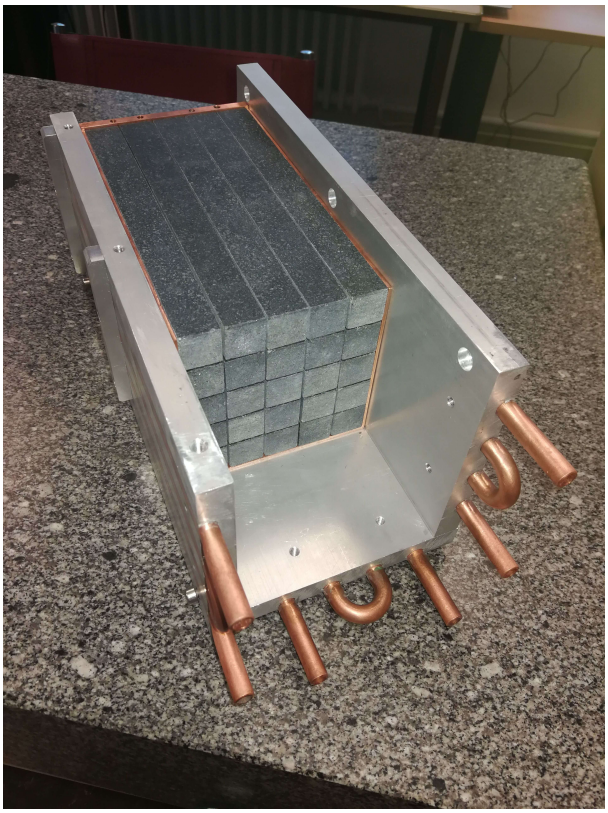

Figure 34: Assembly of the thermal prototype with "fake" crystals made of granite stone

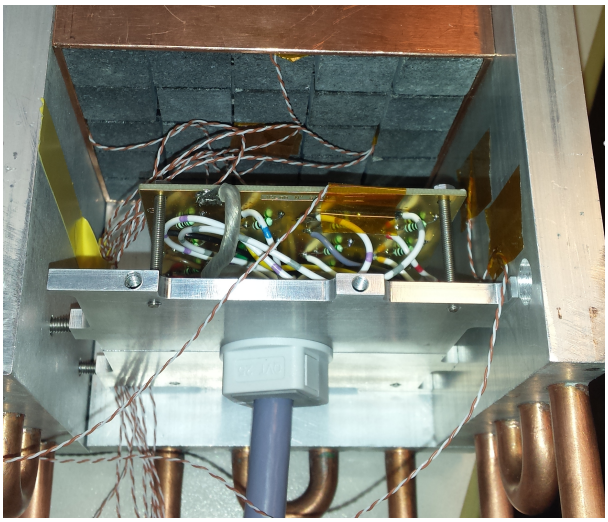

Figure 35: Positioning of the heating PCB in front of the crystals

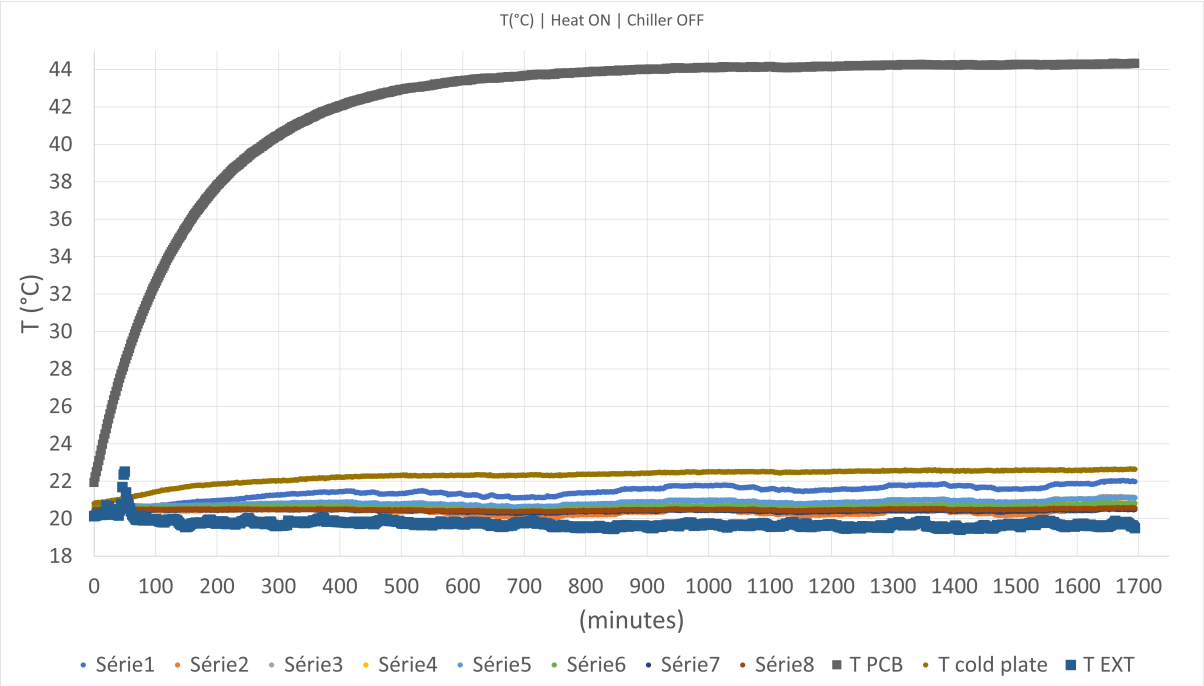

Figure 36: Evolution of the temperature with the heating PCB and without cooling. The gray curve shows the temperature in the heating PCB. The room temperature is shown by the dark blue curve. The light brown curve corresponds to a temperature sensor placed onto the cooling plates. All other curves are the data from different sensors placed along the crystals (see Fig. 38).

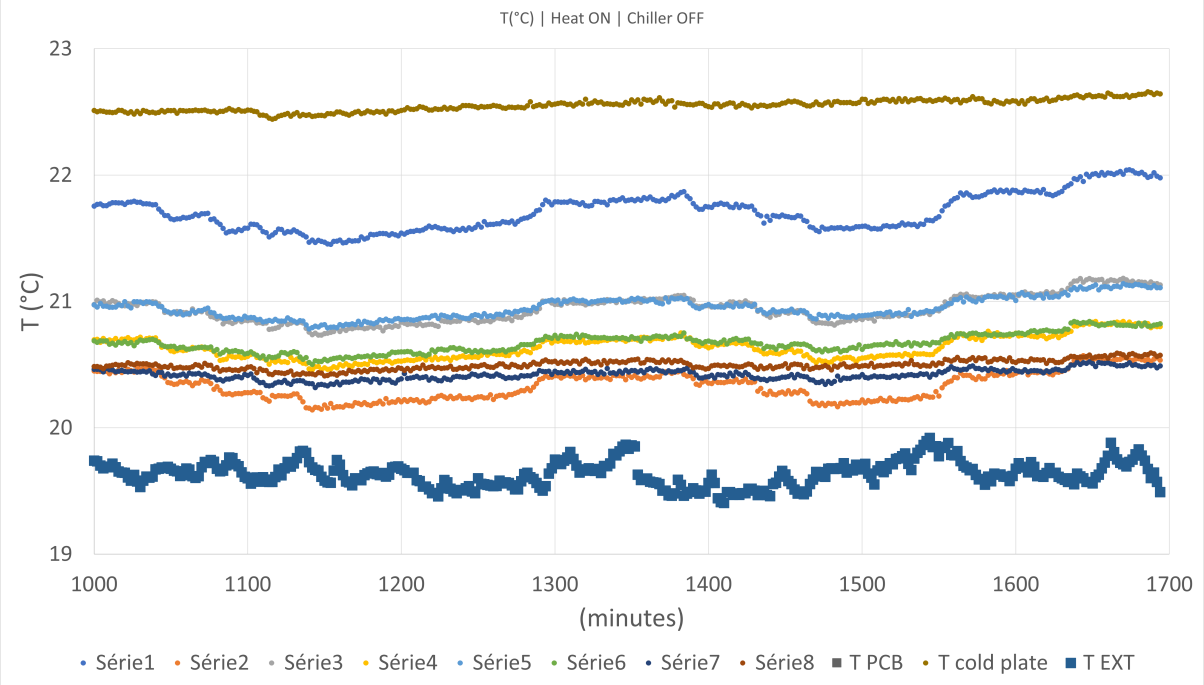

Figure 37: Zoom of Fig. 36 around 19–23 °C in the vertical axis. See legend of Fig. 36 for an explanation of the different curves.

This test demonstrated a temperature stability of 0.5°C at best without active cooling. Therefore, it is clear that cooling must be added to meet the stringent temperature stability requirements. Notably, there was significant variability in temperature readings for sensors located near the PCB, further confirming the necessity of distancing the power source from the crystals to avoid temperature fluctuations. Ensuring this separation will be preferable for achieving the required thermal stability.

4.6.3 Thermal tests with cooling

The second phase of the prototype tests, conducted using "fake" crystals, was performed with the cooling system activated. This stage aimed at evaluating the efficiency of the cooling solution and its impact on thermal stability. The positioning of the thermal sensors used for monitoring is detailed in the Figure 38, ensuring a comprehensive assessment of temperature distribution across the system. The data acquisition system used for the setup is an AGILENT 34972A device. The thermal sensors are thermocouples type T class 1 (Type TX - 1/0.2mm PFA twisted pair extension wires).

The experimental setup used for the thermal tests is shown in Figure 39. Several cases were tested to evaluate the impact of different configurations on thermal stability, including setups with or without heat dissipation from the PCB and with or without the use of a chiller. These tests were conducted in a standard environment rather than a controlled climatic chamber. The ambient temperature varied between 19°C and 27°C. The stability results, evaluated at one sigma, are summarized in Table 4.

Temperature stability with power in front of the crystal and with cooling → ±0.1 °C

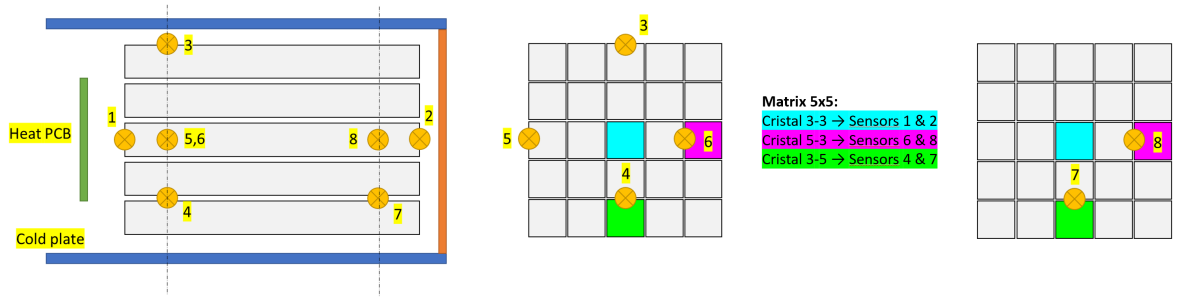

Figure 38: Positioning of the thermal sensors in the prototype

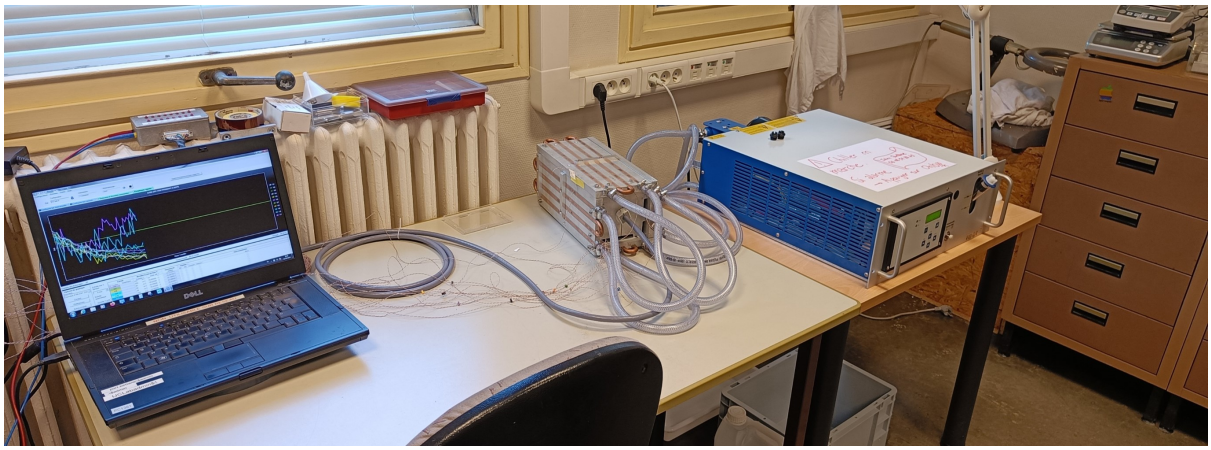

Figure 39: Setup for the thermal measurements in the 5×5 prototype, showing the chiller on the right and the wires from temperature sensors going to the acquisition system (not shown) on the left.

Table 4: Temperature stability for different heating and cooling conditions. The room temperature varied between 19°C and 27°C for different measurements. The values indicate the standard deviation of the temperature variations measured.

	Standard deviation 1 σ										
Results	**101 (C)**	**102 (C)**	**103 (C)**	**104 (C)**	**105 (C)**	**106 (C)**	**107 (C)**	**108 (C)**	**T° pcb**	**T° plate**	**T° ext**
Heat ON - Chiller OFF	0,15	0,11	0,11	0,09	0,09	0,08	0,04	0,04	0,12	0,07	0,09
Heat ON - Chiller ON	0,11	0,08	0,07	0,07	0,06	0,06	0,05	0,05	0,08	0,07	0,26
Heat OFF - Chiller ON	0,05	0,06	0,04	0,04	0,03	0,03	0,02	0,02	0,04	0,03	0,12
Heat ON cycle - Chiller ON	0,57	0,09	0,06	0,07	0,13	0,06	0,08	0,07	8,83	0,65	0,14
Heat OFF - T chiller = 19°C → 0°C	2,05	1,99	1,99	2,06	1,99	2,06	2,04	2,03	1,62	1,90	0,76

The data sheet of the chiller (P302) is given on the the Figure 40.

4.6.4 Thermal analysis on the prototype during the beam test @CERN

For the beam test at CERN the prototype was equipped with 25 PWO crystals. The thermal sensor mapping closely follows the configuration from the previous test, ensuring consistent temperature monitoring throughout the experiment. The test setup is detailed in Figure 41.

The beam test took place during the summer, and the ambient temperature in the experimental hall was significantly high, averaging around 27.5°C ± 1°C. These conditions and their impact on the system thermal behavior are illustrated in the Figure 42 and Figure 43.

The results with the cooling at 19°C show the stability of all sensors remained below 0.1°C

5 Mechanical structure

5.1 Internal structure

A Finite Element Analysis (FEA) model was developed to simulate the mechanical behavior of the internal structure. The model includes 239 crystals stacked on the top of the internal structure, providing a detailed representation of the mass distribution within the assembly (Figure 44). For this initial analysis, copper tubes were not included in the simulation.

The results (Figure 45) show very low deflection and stress levels, well below the elastic limit. This indicates that the structure maintains its mechanical integrity under the expected loads. However, the design remains challenging, as it must integrate the cooling system without compromising structural efficiency. The focus is, therefore, on optimizing the cooling implementation rather than addressing resistance concerns.

5.2 External structure

5.2.1 Mechanical design

The mechanical design of the EEEMCal calorimeter has evolved alongside the development of the Front-End Boards (FEB). The two solutions are on the Figure 46. Several key constraints influence this design:

- **Physics performance:** The geometry and materials are primarily determined by the physics requirements.
- **Clearances with other detectors and the beam pipe:** Sufficient space must be maintained to ensure proper integration without interfering with other detector components.
- **Positioning of the FEB and the Readout System (RDO):** The placement of these elements directly impacts the power dissipation and, consequently, the cooling requirements.

P300 Series Model Overview (Standard Units)

		P302	P307	P310	P312	P315	P320	P330
Cooling Power								
	@ 20°Tw / 20°Ta (Watt)	300	720	900	1150	1620	2400	3500
Tw=Temp Water, Ta=Temp Ambient	@ 20°Tw / 35°Ta (Watt)	170	570	720	930	1210	2100	3000
Temperature Stability	(K)	+/-0.1	+/-0.1	+/-0.1	+/-0.1	+/-0.1	+/-0.1	+/-0.1
	Method of control	Hot gas bypass, PID						
Enclosure	Size (W/D) mm	19" slide-in rack, approx. 640mm deep with external filter on rear						
	Height HU (1HU = 44.5mm)	4	6	6	7	7	9	12
	Noise (Db (A))	< 65	< 70	< 70	< 70	< 70	< 70	< 70
	Weight (Kg) approx.	32	40	42	50	55	65	90
Application Range - Temperature	Coolant water outlet (°C)	10 - 35						
	Ambient (°C)	15 - 40						
	Transportation & Storage (°C)	0 - 70						
Air / water	Fan Ø (mm)	130	200	200	250	250	250	2 x 200
	Air Flow Direction	In through the side panels, expelled out the rear panel						
Water / water	Primary Water (°C)	5 - 25						
	Flow required (l/min)	5 - 10						
	Quality required	Filtered <50µM, < 200mg Chlorine/l						
Water Circuit	Water Filter (externally mounted)	F20	F20 or 5"	F20 or 5"	F20 or 5"	F20 or 5"	F20 or 5"	F20 or 5"
	Filter Grade	Various grades available						
	Air / Water-Water Connections	2x 3/8" stainless steel, internal „G" thread						
	Water / Water-Water Connections	4x 1/2" stainless steel, internal „G" thread						
	Tank Volume (l)	1.8	2	2	2.5	2.5	2.5	2.5
	Water Level Indication	Optical water level display on front panel						
Alarm Interlocks		Alarm contacts (open in alarm state) connected to a 9-pin Sub-D (interlock) on rear panel						
		Alarms available individually or in a collective fault configuration.						
		Both configurations can be brought out to a PC via the RS232 port						
Water Circuit	Flow Sensor	Flow turbine, set point adjustable						
	Default point (l/min)	2	2.5	2.5	2.5	2.5	2.5	2.5
	Water Level Monitoring	Two vertical float switches (warning, alarm)						
	Default High-Low temperature Alarm	15°C Low, 32°C High temperature alarm, (absolute) via Sub-D						
Refrigerant Circuit	High Pressure	18 bar, hysteresis +/- 1bar						
Power Supply	Voltage (VAC)	230VAC +/- 10%, others available						
	Current (A)	2.5	6.5	7	7.5	8	9	9
	Line Frequency (Hz)	both 50and 60						50 or 60
	Power Connections	IEC 950 with line filter						

Figure 40: Datasheet of the chiller P300, the model used for the tests is P302 with PD1 SST pump: flow rate 4l/min at 3.5 bar.

Figure 41: Setup of the beam test @CERN. The 5×5 prototype is represented by the red rectangle in the setup. The chiller is placed on the table, with the AGILENT 34972A device positioned on top of it.

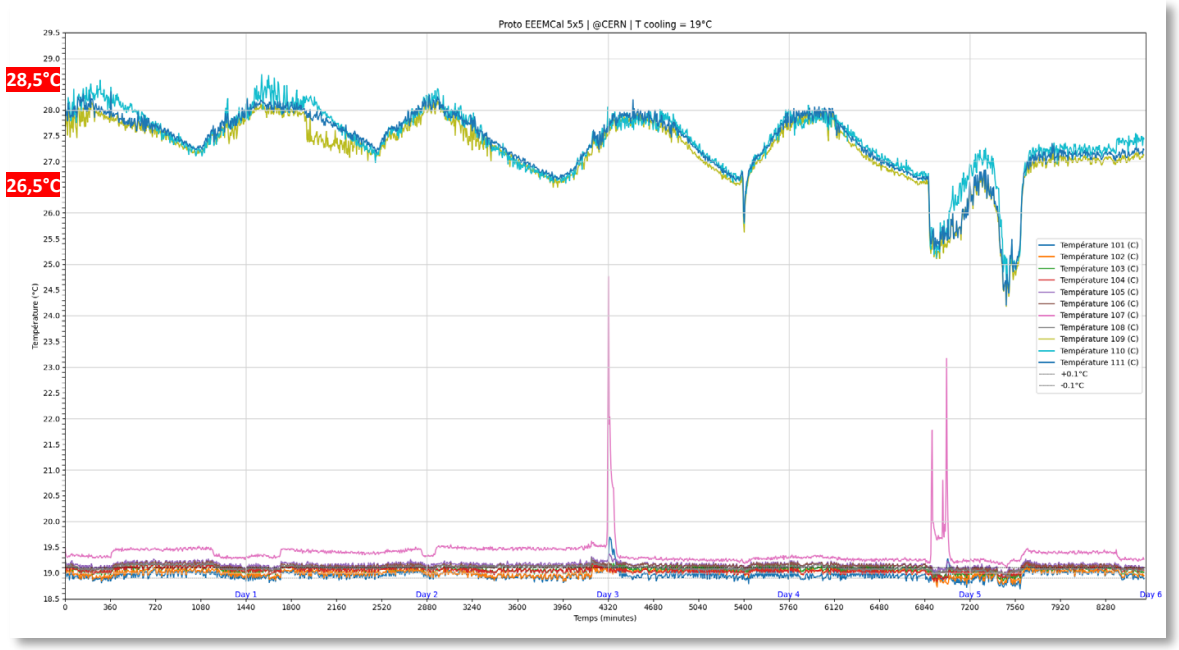

Figure 42: Temperature variation in the room experiment at CERN indicated by the green and blue curves between 26.5 and 28.5 °C. All other curves show the data of temperature sensors placed on the crystals. A zoom of this figure around 19 °C, the operating temperature of the chiller, is presented in Fig. 43.

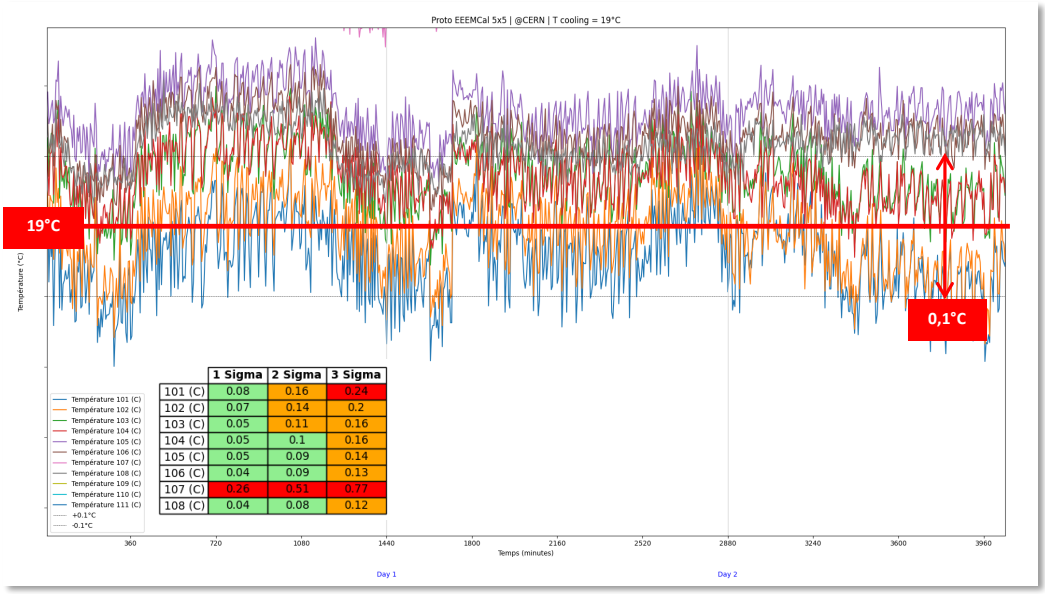

	1 Sigma	2 Sigma	3 Sigma
101 (C)	0.08	0.16	0.24
102 (C)	0.07	0.14	0.2
103 (C)	0.05	0.11	0.16
104 (C)	0.05	0.1	0.16
105 (C)	0.05	0.09	0.14
106 (C)	0.04	0.09	0.13
107 (C)	0.26	0.51	0.77
108 (C)	0.04	0.08	0.12

Figure 43: Temperature stability during the beam test @CERN for different sensors placed on the crystals. Notice that sensor 107 was not working properly (its data, shown in magenta in Fig. 42, are above the vertical scale of this plot).

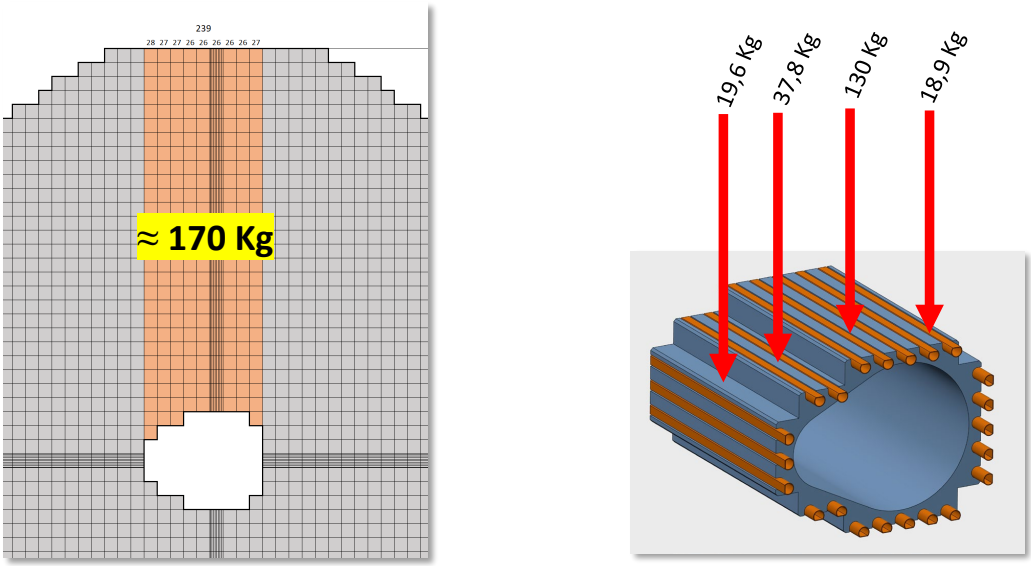

Figure 44: Distribution of the mass on the internal structure

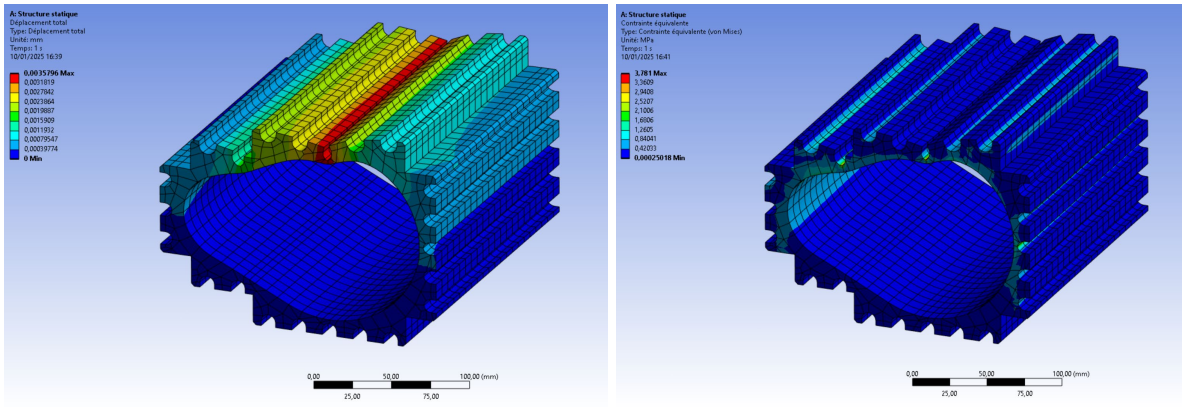

Figure 45: Finite element analysis of the internal structure: deflection (left) and stress (right)

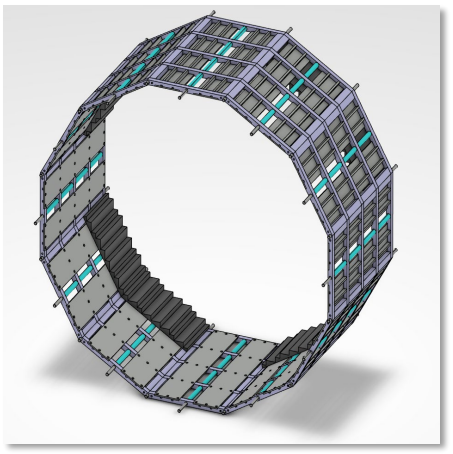

2022

Assembly of rings and plates

-	+
Assembly	Cheap
Cooling	
Stress & Deflection	

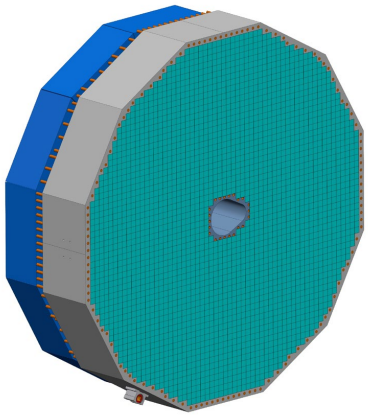

2024

Monobloc

-	+
Expensive	Cooling
Production	Stress & Deflection
Corrosion	No assembly

Figure 46: Evolution of the design of the external structure

When designing the external structure of the EEEMCal calorimeter, two main manufacturing processes are being considered: foundry and machining. Each method has their advantages and challenges:

- **Foundry:** This approach allows for complex geometries and potentially reduces the need for assembly. However, material properties may vary, and additional post-processing might be required to achieve the necessary precision.
- **Machining:** Provides higher dimensional accuracy and better material homogeneity but can be more expensive and time-consuming, especially for large or intricate parts.

A key concern in the cooling system, particularly in the case without copper tubes, is galvanic corrosion. Without proper material selection and surface treatment, corrosion could affect long-term reliability. To address these challenges, an innovative solution using Friction Stir Welding (FSW) is being explored. This technology enables high-quality joints without melting the material, making it a promising alternative for assembling the structure efficiently. The initial quotes suggest that foundry manufacturing is likely not competitive compared to special machining. In both cases, the shape inside the big ring will be realized in machining.

5.2.2 FEA model and hypothesis

The external structure is a key component of the design, as it must ensure both cooling efficiency and mechanical support for all the crystals. Given the weight constraints, the structure must be capable of supporting approximately 2 tons while maintaining mechanical stability. To validate its performance, a Finite Element Analysis (FEA) is conducted to assess its structural integrity under load. This simulation helps to ensure that the design can withstand the expected forces while minimizing deformations and optimizing the material distribution. The results of the FEA will guide potential reinforcements or modifications to improve both thermal management and mechanical strength.

In the worst-case scenario, the structure is fastened at the 3 and 9 o'clock positions, the green parts in Figure 47. This configuration significantly influences the mechanical behavior of the system. The fastening method plays a crucial role in the distribution of stress within the structure. Depending on the attachment points and constraints, it can lead to higher localized stress concentrations, potentially affecting the long-term mechanical integrity.

The calculation process of the external structure involves a step-by-step simulation of the crystals assembly, layer by layer. This approach allows for a detailed evaluation of deflections at each stage, ensuring the precise positioning of all components. Proper alignment is critical, especially for the mounting of the internal structure, where any deviation could impact the insertion of the beam pipe. The central part of the structure supports 665 kg, while the 16 additional surfaces on both sides add 626.5 kg each, from 11.9 kg to 79.8 kg. Each row of crystals exerts a force on the structure. For the central face, there are 59 rows of 17 crystals, following a linear progression. For the other faces, the number of rows varies between 17 and 57, with each row containing either one or two crystals (Figure 48). To guarantee structural integrity during assembly, a total of 59 steps (line of crystals) are planned to systematically monitor and control deflection at each stage. This approach ensures that the final structure meets mechanical and alignment requirements.

The drawing in Figure 49 illustrates the difference between two modeling approaches: the real case, which considers the exact number of crystals on each face, and a simplified model, where

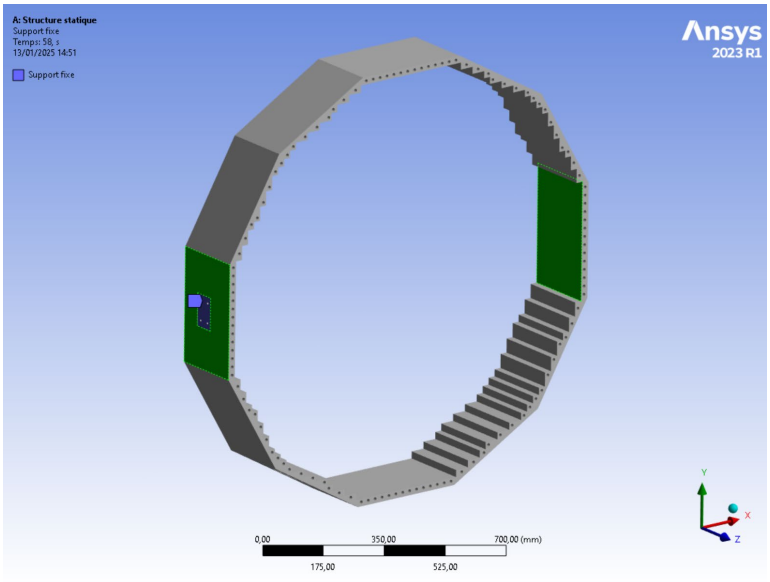

Figure 47: Worst case scenario for the fastening of the EEEMCal, being supported at the 3 and 9 o'clock positions.

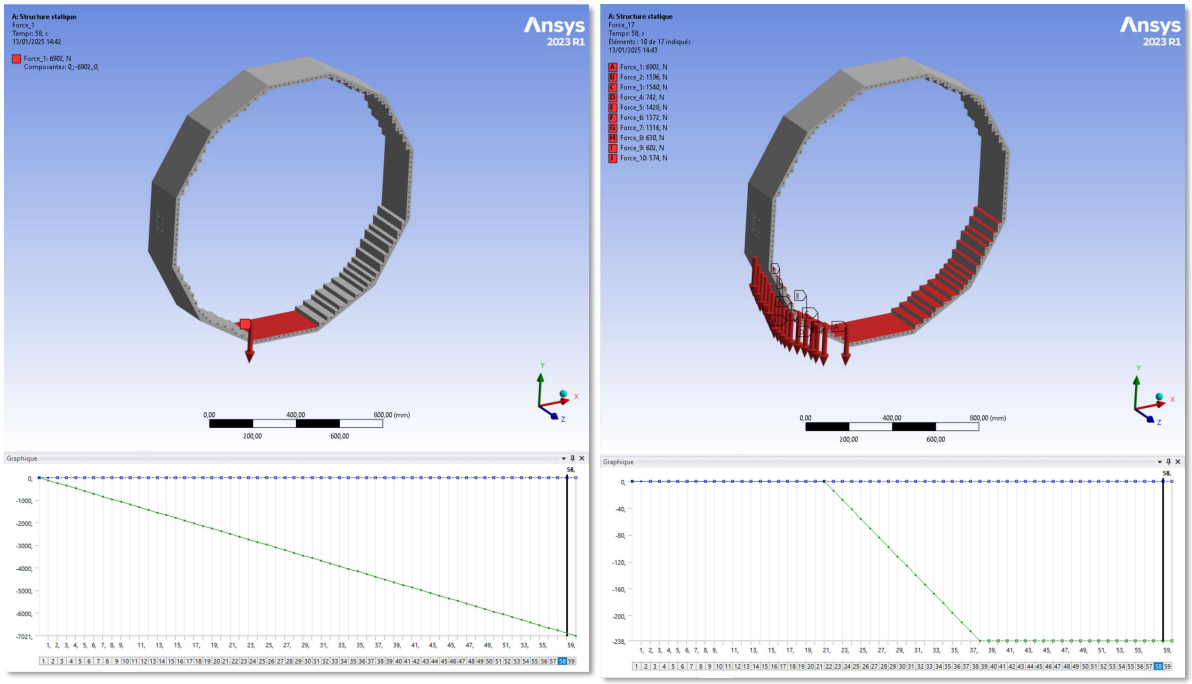

Figure 48: The increase of the forces on the bottom of the external structure of the EEEMCal is illustrated in the figures. The left figure highlights the central face, which supports 665 kg, while the right figure shows the 626.5 kg applied on the left side (indicated by the arrows). Similarly, an additional 626.5 kg is applied on the right side

a uniform distributed force of 2 tons is applied to all faces. The FEA is performed using the real case, ensuring a more accurate representation of the mechanical stresses and deformations within the structure. This approach provides better insight into the actual mechanical behavior, optimizing the design for structural integrity and stability.

5.2.3 Results

The results of the analysis in Figure 50 indicate that the displacement in the X direction is less than 0.5 mm, which does not generate significant stress on the crystals (45 crystals + 0.025). And the displacement in the Y direction reaches a maximum of 0.8 mm in the worst-case scenario, while for step 26, just before the assembly of the internal structure, it is 0.36 mm.

The results of the stress depend on the mechanical solution used to fasten the calorimeter. In cases where the fastening surface of the rails area is small, the stress levels become unacceptable. This indicates that a larger contact surface or an alternative fastening method may be required to ensure the structural integrity and mechanical stability of the system (Figure 51), highlighting the need for an optimized fastening approach that can distribute the forces more evenly and reduce the stress on the structure. This could involve adjustments to the mounting method or surface area to ensure the mechanical solution remains effective without compromising the integrity of the system.

5.2.4 Enhancement

To improve the mechanical design and reduce stress and deflection, the following steps are proposed:

- **Improve the fastening method:** Focus on enhancing the way the mechanical structure is fastened to ensure better load distribution and minimize localized stress.
- **Increase surface area:** Use a larger surface area to help distribute the forces more evenly, which can reduce both stress and deflection by nearly a factor of 2.
- **Positioning on rails:** Place the calorimeter on rails positioned at the 5 o'clock and 7 o'clock positions, the green circles in the Figure 52. This will help reduce displacement and stress by stabilizing the structure.

5.2.5 Construction & procurement

There is currently active work focused on developing a method to build the external structure as a single block. This effort is divided into two main parts:

- **Fabrication of the block:** Two options are being considered for the fabrication of the structure: machining or foundry. Regardless of the method chosen, machining will still be necessary to create all the precise faces required for the accurate placement of the crystals.
- **Cooling inside the structure:**: In parallel to the fabrication, two prototypes will be constructed to compare the efficiency of two different cooling methods: cooling with copper

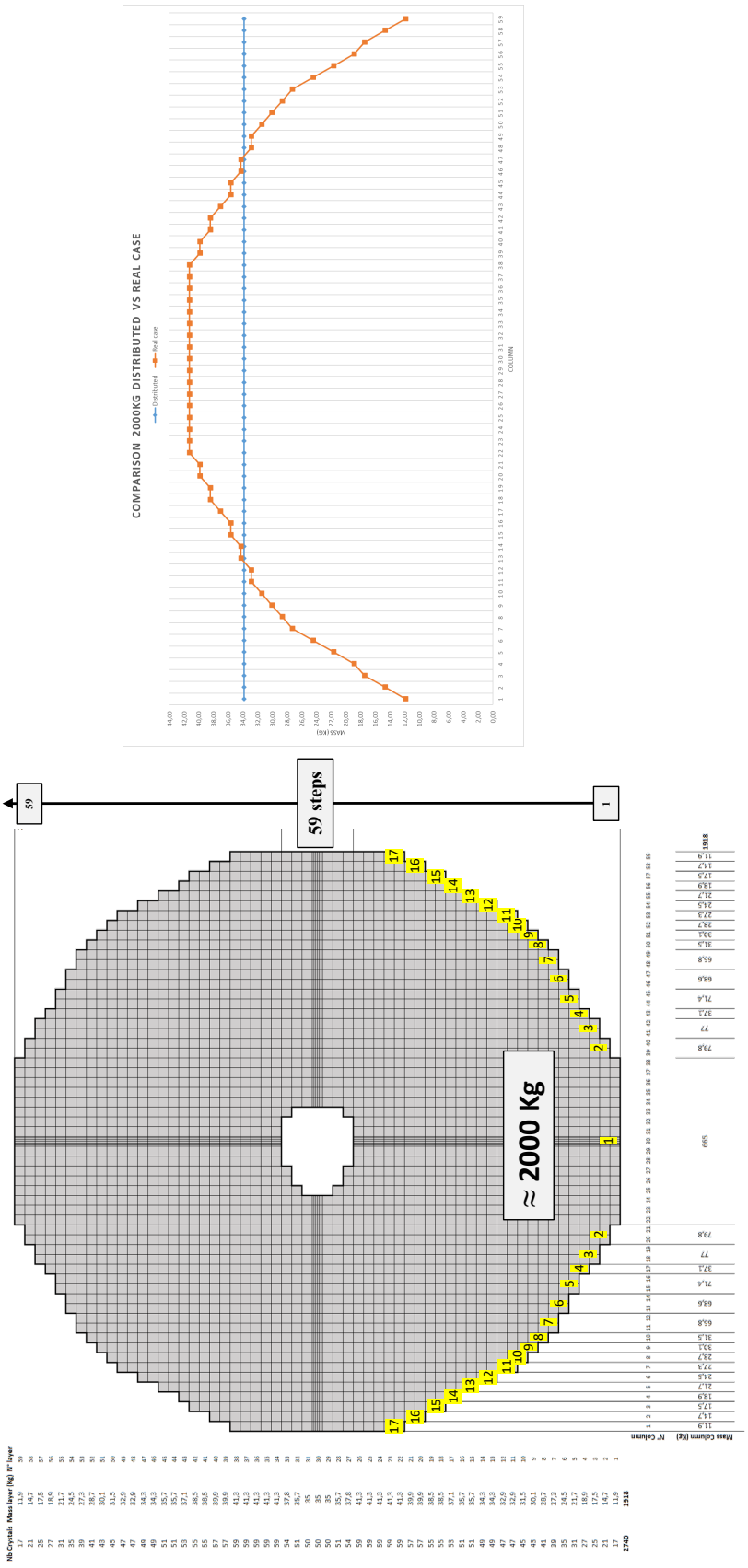

Figure 49: Distribution of the mass on the external structure, comparison between distributed force and real case

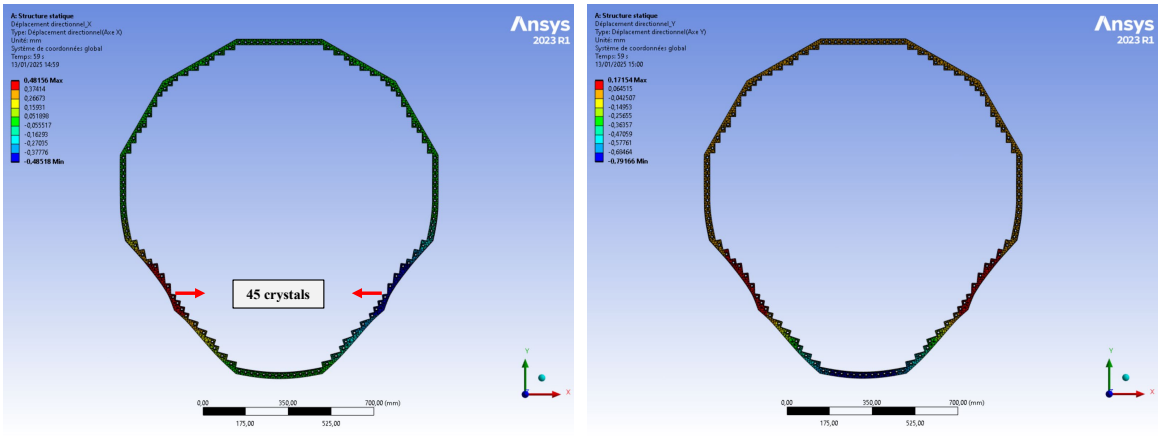

Figure 50: FEA: deflection and stress on the external structure of the EEEMCal

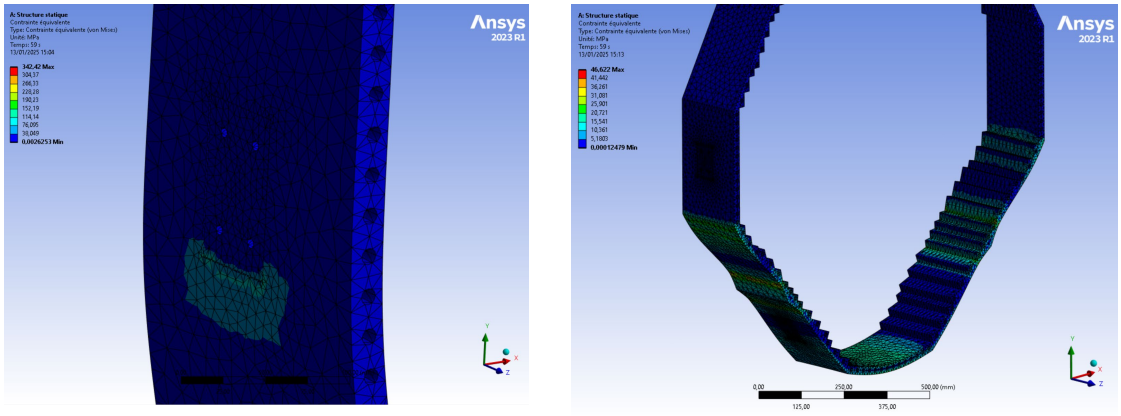

Figure 51: The FEA model initially used a small fixed surface, as shown in the left figure, which resulted in excessively high stress levels. In contrast, the right figure presents the results when the entire surface is fixed in the ANSYS model, leading to a significant reduction in stress. This demonstrates the importance of optimizing the boundary conditions to achieve a more realistic and structurally sound design.

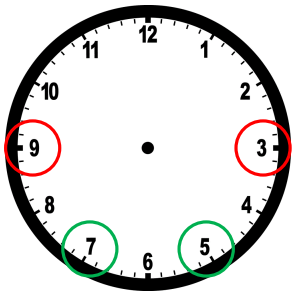

Figure 52: Location for the positioning of the rails. Red: worst case. Green: Less stress and deflection.

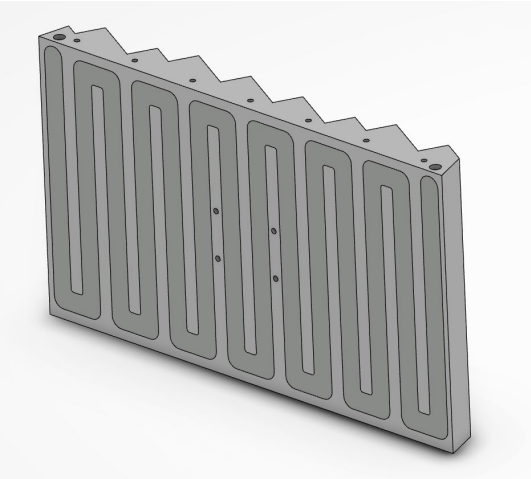

Figure 53: Design of the prototype using FSW technology

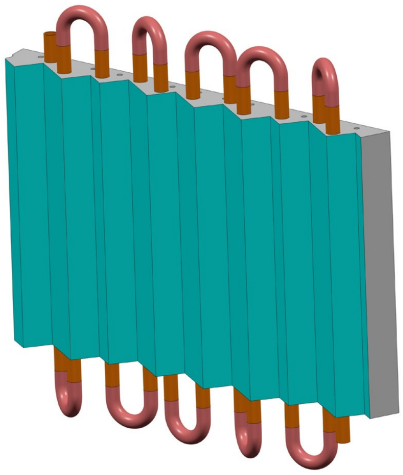

Figure 54: Design of the prototype with copper tubes

tubes and cooling with FSW (Friction Stir Welding), technology using a machined coil. Each prototype will be designed with only 1/12 of the entire structure to evaluate their effectiveness on a smaller scale (Figure 53 and Figure 54).

6 Mechanical assembly

6.1 Crystals assembly procedure

The assembly procedure (Figure 55) follows a well-structured sequence to ensure precision and quality at each step. The process begins with the assembly of the crystals, where each crystal is carefully positioned and prepared. Prior to assembling the internal structure, a control check is performed to ensure all components meet the required specifications. Once the crystals are in place, the internal structure is positioned accurately, followed by a thorough control after the assembly to confirm the alignment of the structure.

Next, the assembly of the crystals is completed, and the grid is fastened and will securely hold the PCBs in place. An optical coupling is then performed between the SiPM PCB and the crystal. A quality control check (with the naked eye) is conducted from the front side of the

system to verify the accuracy of the optical coupling.

The assembly progresses with the installation of the electronic boxes along with insulation on the back side and the copper plate on the front to provide proper cooling and structural support. Following this, the cabling and tubing are installed to ensure the system is fully connected and operational. Finally, the integration of all components is completed, ensuring that the entire system is ready for testing and operation. Each phase of the assembly is carefully monitored for quality to guarantee the final system performs to specifications.

6.2 List of materials and equipment, geographical location

The materials to be installed for the project include the crystals, the mechanical structures (both internal and external), a grid for fastening the PCB, copper plates with insulation, the cooling system, and electronic boxes with cables. The crystals are located in the USA, while the mechanical structures and cooling components are situated in France. The transportation of these materials will be handled by plane, in flight cases, to ensure safe and efficient delivery.

Regarding the assembly process, two options are being considered:

- Assembly at Jefferson Lab (JLab) and transport to BNL
- Assembly at BNL

These two options aim to balance the complexity of the installation process with the logistical considerations and the specific requirements of each site. The available resources will play a key role in determining the most suitable assembly approach.

In both cases, a pre-assembly of the mechanical structure will be carried out in the mechanical workshop at IJCLab. The main objectives are to ensure the proper assembly of all mechanical components and, if possible, to validate and characterize the cooling systems. This step will help identify potential integration issues early and optimize the final assembly process.

Some tasks can be carried out in parallel with the mechanical assembly, such as the wrapping of crystals. To ensure the required quality, a procedure and training by experts will be necessary. Additionally, the assembly of the Front-End Boards (FEB) and their mechanical components should be prepared as much as possible in advance to minimize assembly time in the experimental hall and optimize the overall installation process.

6.3 Resources required

The resources needed for this project will be discussed with the collaboration team to ensure that all necessary materials, tools, and expertise are available. This includes determining the specific requirements for each phase of the project, such as fabrication, assembly, and testing, as well as identifying any additional support or equipment needed from the partners. This involves packaging and securing the components to ensure safe transport and handling during shipment. The goal is to efficiently manage resources and time while ensuring the components arrive in optimal condition for assembly.

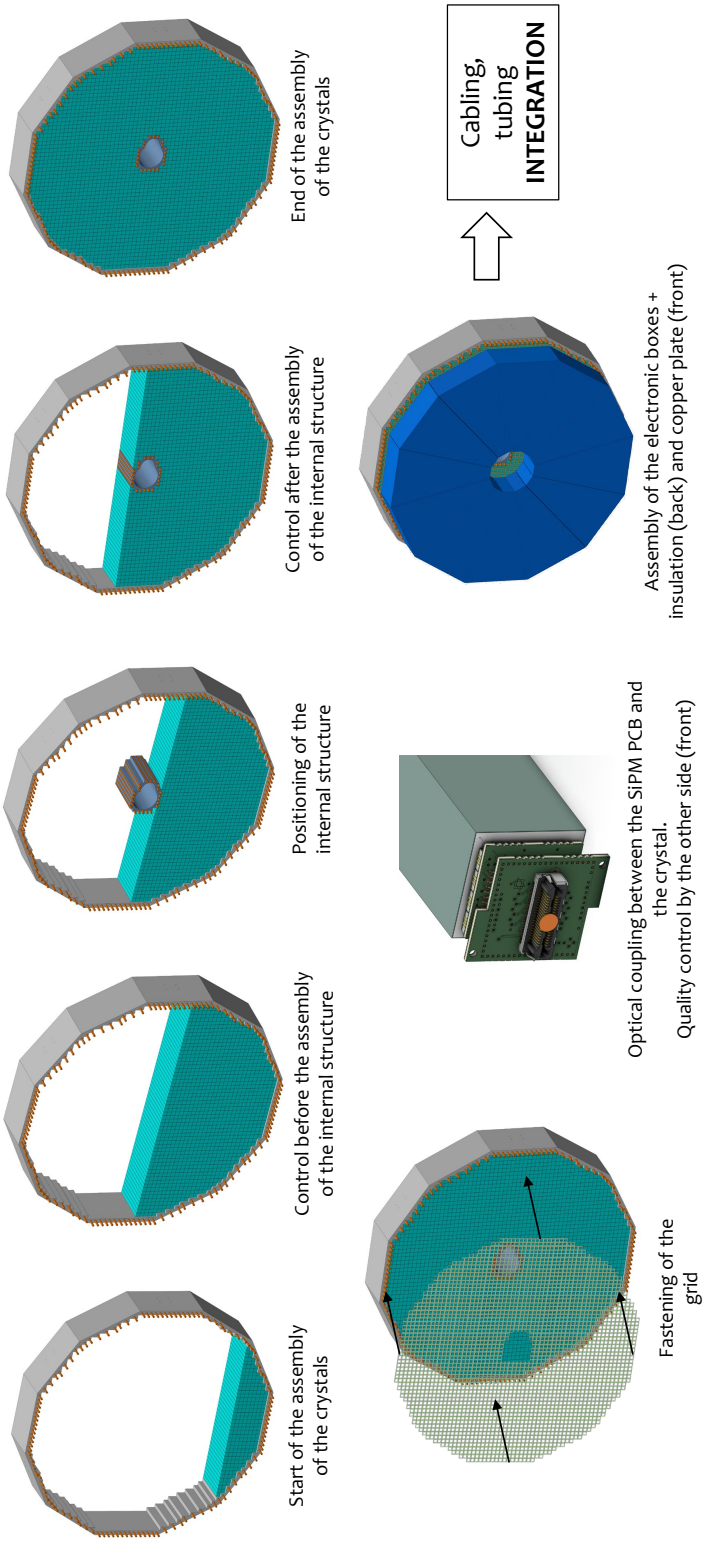

Figure 55: Assembly of the crystals step by step

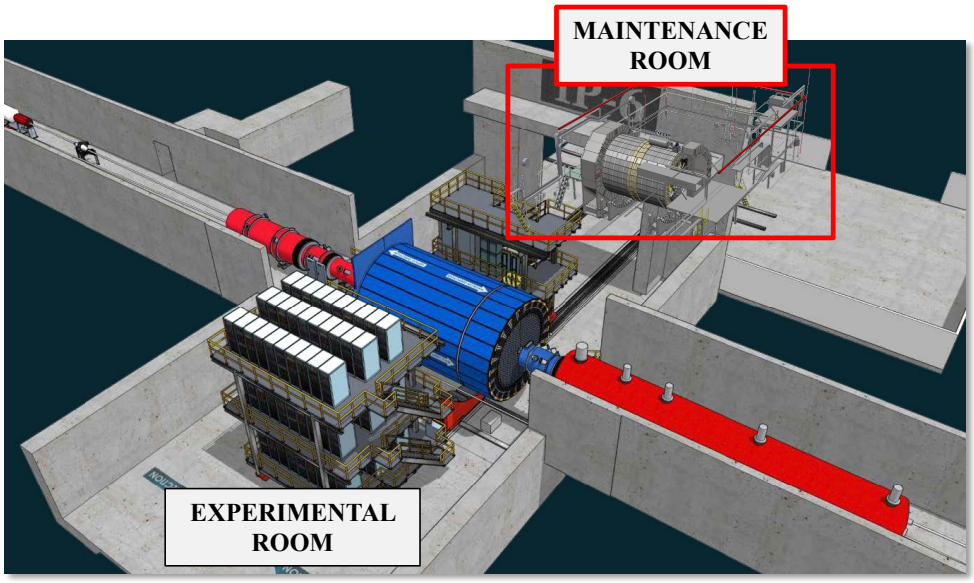

Figure 56: Overview of the experimental room and the maintenance room

7 Installation

7.1 Place for the installation

The installation in the maintenance room (Figure 56) requires careful planning and execution to ensure a smooth and efficient process. A work platform will be necessary to provide a stable and elevated working surface for assembly and positioning of components, ensuring ease of access to all areas. The CAD of the work platform is visible in Figure 57. In addition, special tooling will be required for precise inserting and handling of the EEEMCal, as standard tools may not be sufficient for the task. A bridge crane will also be needed for lifting and positioning the heavy components safely, allowing for alignment and installation within the maintenance room.

7.2 Installation procedure

The installation procedure follows a precise set of steps to ensure the proper placement and alignment of the detector:

- Position the detector onto a tooling using the bridge crane to ensure safe handling and accurate placement.
- Fasten the temporary rails to stabilize the detector and facilitate its movement into the desired position.
- Slide the detector carefully into the carbon tube, ensuring it is aligned correctly and securely within the tube.
- Once the detector is in place, remove the temporary rails to complete the installation and prepare the system for the next steps in the setup process.

A conceptual design of the setup for the installation is detailed in Figure 58.

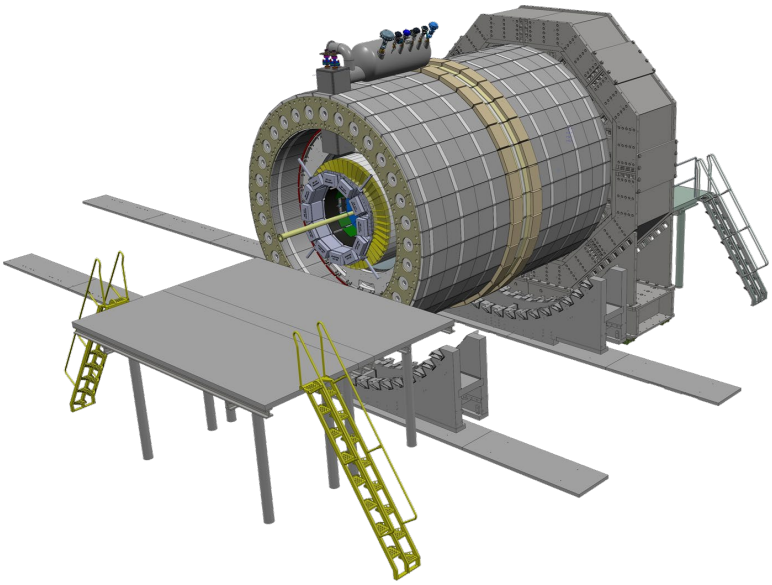

Figure 57: Overview of the platform to perform the installation (design in progress)

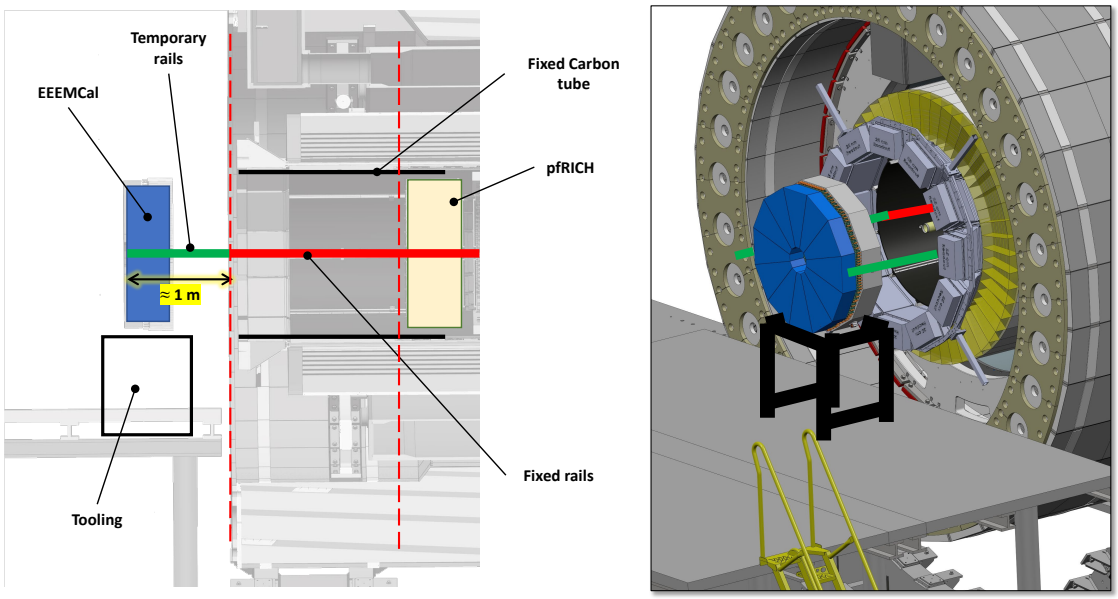

Figure 58: Installation procedure to install the EEEMCal

7.3 Special tooling

Special tooling is required for the insertion of the EEEMCal (and pfRICH) into the system. BNL is responsible for the design and fabrication of this tooling, ensuring it meets the necessary specifications for the precise handling and positioning of the components. The concept of the tooling needs to be validated by both the EEEMCal team and the BNL staff to ensure it aligns with the requirements and expectations from both sides. This critical point will be discussed during the "3I" meetings with the chief coordinator, Rahul Sharma, to ensure all stakeholders are aligned and the tooling design is approved for fabrication and use in the installation process.

7.4 Integration of the detector (services, cooling, FEB, RDO, DAQ)

The installation of cables and services is a critical part of the setup, ensuring proper functionality and communication between the components. LED cables will be installed, with one LED per crystal, controlled by the FEB. Additionally, thermal sensor cables will be installed for approximately 10% of the crystals, with two sensors per crystal, totaling around 600 cables. Signal cables will also be integrated, the quantity of which depends on the grouping configuration—whether the system uses 16 SiPMs or 4 SiPMs per readout. Finally, power supply cables will be routed to ensure all components receive the necessary electrical power.

Currently, there is only a preliminary estimate of the services, as shown in Figure 59. It is important to have a representative estimate of the cables needed for the EEEMCal, as this will inform the design and organization of the installation. The area currently being used must be carefully consolidated to accommodate the required cable routing, power supplies, signal connections, and other services while maintaining proper organization and accessibility.

8 Safety

8.1 Risk analysis

Table 5 presents a list of identified risks, together with their associated level of criticality and probability.

8.2 Magnetic field and dew point

The presence of a strong magnetic field in the experiment area requires careful selection of cooling system components, particularly fans and heat exchangers. Standard fans with ferromagnetic parts may experience performance degradation or even failure due to magnetic forces affecting their motor operation. Therefore, it is crucial to use magnetically shielded or non-magnetic fans to ensure reliable cooling. Similarly, heat exchangers must be designed to avoid magnetic interference, ensuring that their structural integrity and efficiency are not compromised. Additionally, in the event of a quench—when the superconducting magnet transitions to a normal resistive state—there can be a rapid and intense change in the magnetic field, potentially inducing high currents and forces on conductive parts. This scenario must be considered when designing the cooling system to prevent mechanical damage or malfunctions.

Maintaining the temperature of cooling elements above the dew point is essential to prevent condensation, which could lead to electrical failures and corrosion. In a high-humidity environment, a poorly controlled cooling system can cause moisture to accumulate on cold surfaces, such as pipes, heat exchangers, or electronic components. To avoid this, temperature and humidity sensors should be used to monitor conditions, and insulation should be applied to cold

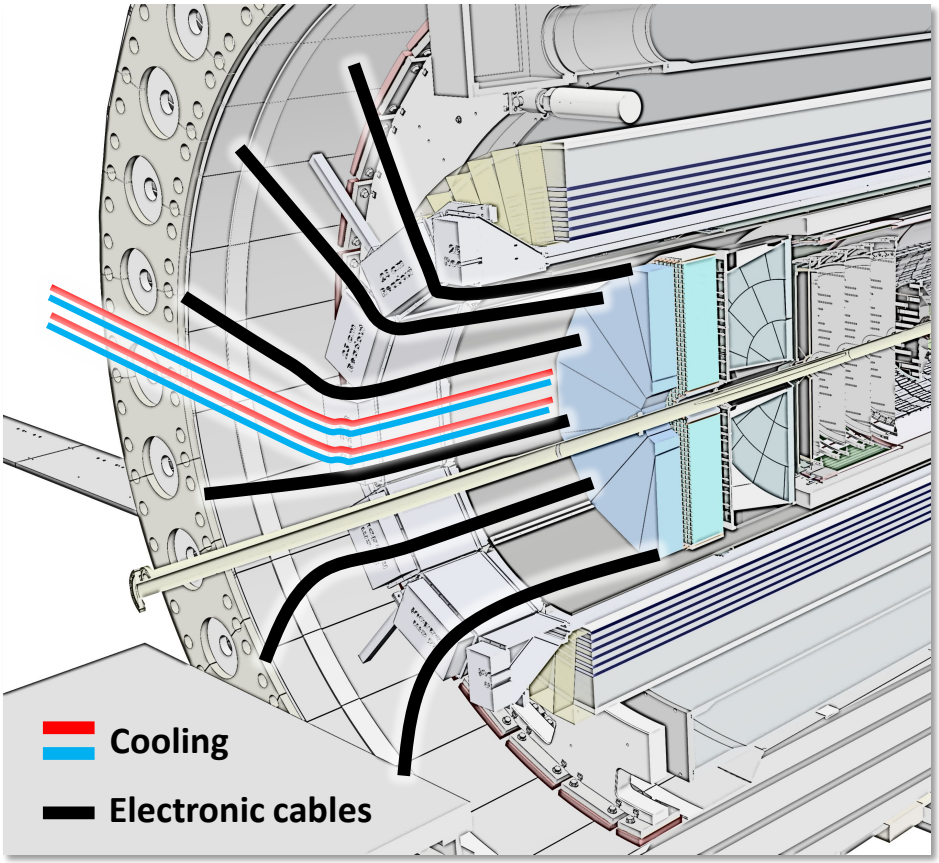

Figure 59: Sketch of the services for the EEEMCal

Table 5: Table of the risks analysis

N1	Risks identified	Description	Effects	Category	Probability	GravitéGravity	Criticity %	Criticity	Mesure(s)
1.	Structural failure	Poor design or inappropriate material selection for the crystal supports or overall structure	Damage to PWO crystals, performance loss, repair or replacement of structural parts	Mechanical / Design	**2 - low (unlikely)**	**4 - High**	32%	Elevé	- Conduct detailed structural analysis and simulation tests. - L(1)C
2.	Mechanical incompatibility of sub-assemblies	Inadequate mechanical tolerances or poor integration between subsystems	Misalignment, assembly difficulties, performance degradation	Mechanical / Assembly	**3 - Medium (possible)**	**4 - High**	48%	Elevé	- Implement strict quality control on mechanical tolerances. - Ensure collaborative design reviews between teams.
3.	Vibrations or thermal stress	Environmental vibrations or thermal expansion of materials	Cracks in the crystals, mechanical fatigue, degradation of stability and precision	Environment / Mechanical	**2 - low (unlikely)**	**4 - High**	32%	Elevé	- Design shock-absorbing and vibration-damping systems. - Use materials with suitable thermal expansion coefficients.
4.	Premature wear of mechanical components	Repeated mechanical loads, harsh conditions, or poor material choice	Unplanned maintenance, component replacement, operational downtime	Materials / Operating conditions	**2 - low (unlikely)**	**2 - low**	16%	Faible	- Choose materials with high durability under operating conditions. - Schedule regular inspections and maintenance.
5.	Interference with electronic systems	Poor management of space between mechanical and electronic components	Electronic signal malfunctions, disruptions, need for repairs	Electromechanical Integration	**3 - Medium (possible)**	**4 - High**	48%	Elevé	- Ensure proper spacing and shielding between mechanical and electronic components.
6.	Inefficient cooling	Inadequate design or installation of cooling systems	Overheating of electronic components, performance degradation	Thermal / Mechanical	**3 - Medium (possible)**	**5 - Very high**	60%	Critique	- Optimize cooling system design, conduct thermal simulations. - Regularly monitor and maintain cooling systems.
7.	Mechanical assembly errors	Human errors or lack of clear procedures for assembling components	Incorrect assembly, delays, need for re-assembly of parts	Assembly process	**3 - Medium (possible)**	**2 - low**	24%	Moyen	- Develop clear assembly procedures and ensure proper training for assembly teams. - Use precision tools for assembly.
8.	Contamination or damage during manufacturing	Contamination or damage during the manufacturing or handling of sensitive components (crystals, supports)	Deterioration of optical components (PWO), alteration of light collection, reduced performance	Manufacturing / Handling	**2 - low (unlikely)**	**2 - low**	16%	Faible	- Implement cleanroom procedures for sensitive components. - Use protective handling methods and specialized equipment.
9.	Damage during transport	Insufficient protection or improper packaging of components during shipping	Breakage of SiPMs or crystals, misalignment, need for re-calibration, delayed delivery	Transportation / Packaging	**3 - Medium (possible)**	**5 - Very high**	60%	Critique	- Use shock-proof and vibration-resistant packaging. - Implement real-time monitoring during transit (e.g., GPS sensors).
10.	Galvanic corrosion	The aluminum structure could be subject to galvanic corrosion due to the material difference in the connectors.	This can degrade the efficiency of the cooling system and accelerate material wear over time.	Mechanical / Cooling	**4 - High (probable)**	**5 - Very high**	80%	Critique	- Use shock-proof and vibration-resistant packaging. - Use other liquid for the cooling and use chemical products
11.	Exposure to environmental conditions during transport	Exposure to moisture, temperature fluctuations, or shocks during transportation	Degradation of sensitive components (SiPM, PWO), mechanical or optical defects, overall system performance issues	Transportation / Environmental	**3 - Medium (possible)**	**5 - Very high**	60%	Critique	- Use temperature and humidity-controlled containers. - Choose transport routes and methods minimizing exposure risks.

surfaces. If necessary, dehumidification systems can be implemented to lower ambient humidity and minimize the risk of condensation-related issues.

8.3 Preventive measures

To mitigate the mechanical and transportation-related risks identified in the project, several preventive measures can be implemented. For structural integrity, detailed structural analysis and simulation tests should be conducted, ensuring the use of appropriate materials for load-bearing components. To address mechanical incompatibility between sub-assemblies, strict quality control on mechanical tolerances and collaborative design reviews between teams are essential. Vibration and thermal stress can be mitigated by designing shock-absorbing and vibration-damping systems, as well as selecting materials with appropriate thermal expansion properties. Regular maintenance and inspections, along with the use of durable materials, will help prevent premature wear of mechanical components. Shielding and proper spacing between mechanical and electronic components are critical to avoid interference with electronic systems, while efficient cooling can be ensured by optimizing the design and regularly monitoring the cooling systems. Furthermore, assembly errors can be minimized by developing clear procedures and providing proper training to assembly teams, with the use of precision tools. To prevent contamination or damage during manufacturing, clean-room procedures, and protective handling methods should be enforced. Regarding transportation, protective packaging that is shock-proof and vibration-resistant is necessary to prevent damage during transit. Additionally, temperature and humidity-controlled containers should be used to safeguard components from environmental exposure, and transport routes and methods should be carefully chosen to minimize risks. These measures together form a comprehensive approach to ensuring the mechanical reliability and safe transportation of critical components in the project.

8.4 Compliance with standards

Ensuring compliance with safety and engineering standards is very important for both the transportation and installation of the 2.5-ton detector in the experimental hall. During transportation, it is essential to follow international shipping regulations, including shock and vibration resistance standards (such as ISO 13355 or ASTM D4169) to protect sensitive components. Proper packaging and securing in flight cases should ensure safe handling and avoid mechanical stress. For the installation phase, industrial lifting and handling standards should be followed. The installation should also comply with workplace safety regulations. Adhering to these standards will minimize risks, protect equipment integrity, and ensure a smooth and safe installation process.

Generally, compliance with BNL requirements and standards will be necessary.

9 Development plan

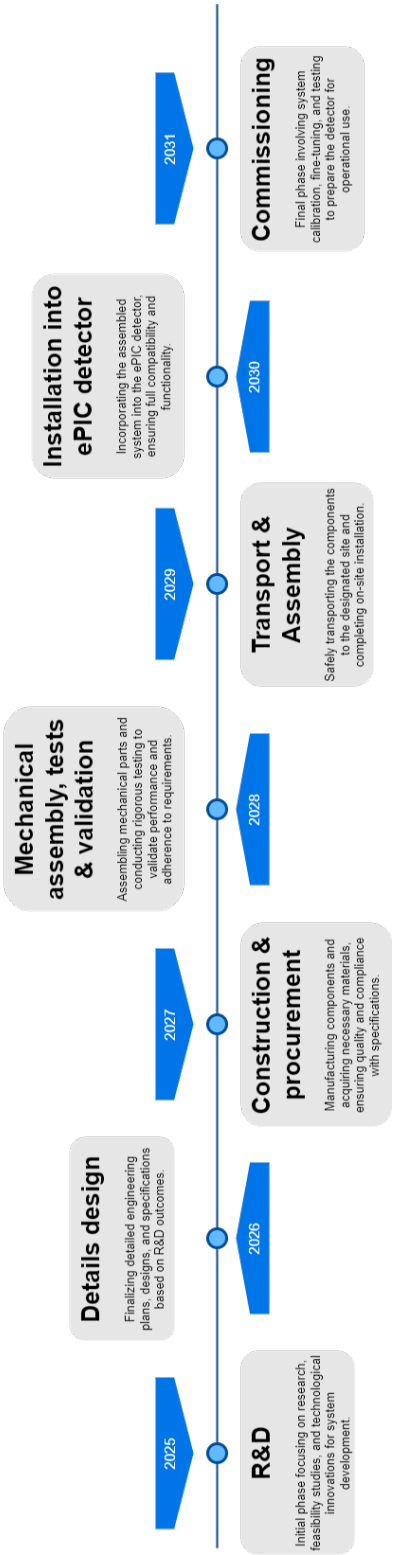

Figure 60: Overall view of the schedule and main phases

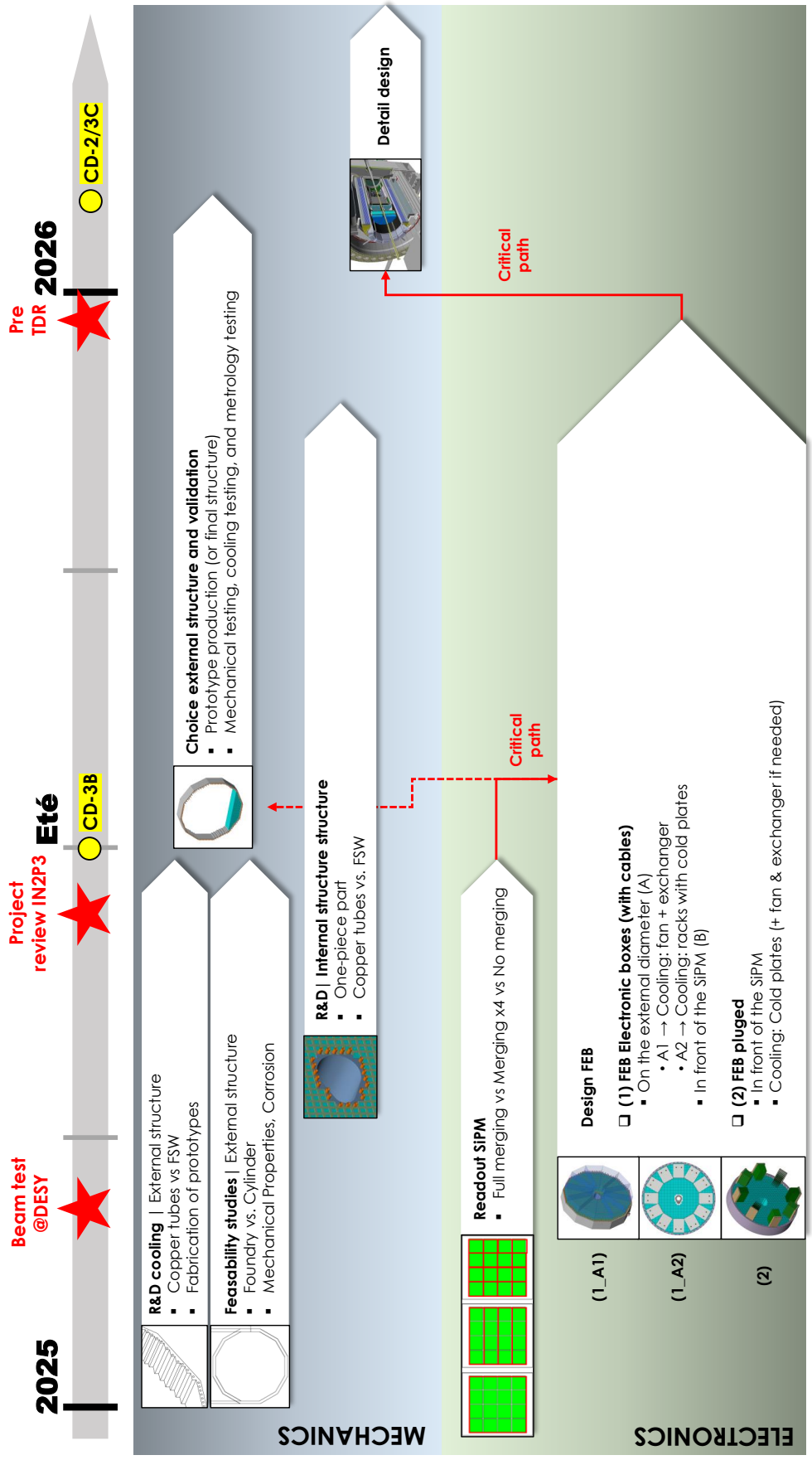

Figure 61: Tasks planned for the year 2025

List of Figures

List of Tables

References

[1] R. Abdul Khalek et al. Science Requirements and Detector Concepts for the Electron-Ion Collider: EIC Yellow Report. *Nucl. Phys. A*, 1026:122447, 2022.

[2] T. Horn et al. Scintillating crystals for the Neutral Particle Spectrometer in Hall C at JLab. *Nucl. Instrum. Meth. A*, 956:163375, 2020.

[3] Mitsuru Ishii, Kenji Harada, Masaaki Kobayashi, Yoshiyuki Usuki, and Tatsuya Yazawa. Mechanical properties of PbWO-4 scintillating crystals. *Nucl. Instrum. Meth. A*, 376:203–207, 1996.

[4] Lorenzo Scalise, Daniele Rinaldi, Fabrizio Davi, and Nicola Paone. Measurement of ultimate tensile strength and Young modulus in LYSO scinti llating crystals. *Nucl. Instrum. Meth. A*, 654:122–126, 2011.

[5] D. Kalinkin. New geometry implementation, 2024. https://indico.bnl.gov/event/25996/.

[6] R. Wimmer. Forward endcap acceptance; beam-pipe constrains, 2024. https://indico.bnl.gov/event/27193/.

[7] T. Horn. EIC Detector Geometry, 2024. https://eic.jlab.org/Geometry/Detector/.

[8] L. Schmitt (GSI Darmstadt) F. Sefkow (DESY Hamburg) R. Novotny (JLU Gießen), R. Pöschl (IJCLab Orsay). EIC Project detector technical review of the electromagnetic and hadronic calorimetry, 2022. https://indico.bnl.gov/event/17721/, TR2022ECalHCal.

[9] C. Muñoz Camacho. Cooling for the backward ECal, 2024. https://indico.bnl.gov/event/21650.